FISHERIES OCEANOGRAPHY

FISHERIES OCEANOGRAPHY Fish. Oceanogr. 18:4, 201–223, 2009

Simulation of physically mediated variability in prey resources of a larval fish: a three-dimensional NPZ model

S. HINCKLEY,[1,*] J. M. NAPP,[1] A. J. HERMANN[2] AND C. PARADA[2]

[1]*Alaska Fisheries Science Center, 7600 Sand Point Way NE, Seattle, WA 98115, USA*

[2]*Joint Institute for the Study of Atmosphere and Oceans, University of Washington, Seattle, WA 98195, USA*

ABSTRACT

A three-dimensional biophysical nutrient–phytoplankton–zooplankton model was used to investigate the spatial and temporal dynamics of food resources for young walleye pollock in the western Gulf of Alaska, to further understanding of recruitment processes for pollock. We modeled nitrogen, phytoplankton, a large herbivorous grazer parameterized as *Neocalanus* spp. (the biomass dominant copepod in the Gulf), and the 13 stages (egg, naupliar and copepodite) of *Pseudocalanus* spp. (a major constituent of the diet of pollock) so that the appropriate size class of food for each size of larval pollock was represented. Model results identified an area between the Semidi and Shumagin Islands that may not be suitable as a nursery area early in the year due to low prey abundance. Modeled mesoscale eddies, previously hypothesized to be important for larval pollock retention in Shelikof Strait, contained higher prey concentrations than the surrounding waters when they were cyclonic. This work also help to understand the consistency of pollock spawning in time and space in Shelikof Strait, by examining the timing and location of prey availability which, along with transport, narrows the window for optimal spawning.

Key words: biophysical models, nutrient–phytoplankton–zooplankton models, prey dynamics, recruitment, *Theragra chalcogramma*, walleye pollock

INTRODUCTION

Walleye pollock (*Theragra chalcogramma*) supports one of the largest single species fisheries in the world, with major stocks in the Bering Sea and the Gulf of Alaska. A large population of pollock spawning in Shelikof Strait, Gulf of Alaska (Fig. 1), was first seen in the early 1980s, when stock levels were high (~1.0 million tons) in this region. Biomass levels have declined since then (to ~145 000 tons; Dorn *et al.*, 2007), but the population is still important for both the fisheries and the endangered Steller sea lion (which feeds on pollock) (Merrick *et al.*, 1997).

Recruitment variability of pollock in this region is high (Megrey *et al.*, 1995; Bailey and Ciannelli, 2007), and survival during the larval period has been identified as critical. An early hypothesis about successful recruitment of pollock spawned in Shelikof Strait was that transport along the Alaska Peninsula was necessary to move young fish to a nursery area near the Shumagin Islands, and that transport offshore or into the Alaskan Stream would result in starvation and loss of animals to the population. It has also been hypothesized (Canino *et al.*, 1991; Bograd *et al.*, 1994; Stabeno *et al.*, 1996; Napp *et al.*, 2000) that entrainment into mesoscale eddies may be beneficial for larvae, either because eddies promote retention and eventual transport to favorable nursery areas (Hermann *et al.*, 1996), or because food supplies may be greater in the eddies.

Since the late 1980s, the 'critical stage' at which recruitment is set may have shifted to the juvenile stage for Gulf of Alaska pollock (Bailey, 2000; Bailey and Ciannelli, 2007). This may be due, in part, to top-down processes, such as increasing predation pressure on juvenile fish (Bailey, 2000; Hollowed *et al.*, 2000; Ciannelli *et al.*, 2004). Regardless of whether it is bottom up, top-down or a combination that determines year-class strength, good larval survival is a necessary condition of good recruitment (Bailey and Spring, 1992). High rates of larval survival are likely dependent on nutritional resources, both prey quantity (Canino *et al.*, 1991) and prey quality (Davis and Olla, 1992).

A better understanding of biophysical effects on feeding conditions for larval pollock should aid in understanding causes of recruitment variability, which would significantly increase the effectiveness of stock management. It would also potentially allow

*Correspondence. e-mail: sarah.hinckley@noaa.gov

Received 3 October 2007

Revised version accepted 3 March 2009

doi:10.1111/j.1365-2419.2009.00505.x

Figure 1. The western Gulf of Alaska and Shelikof Strait. Line 8 can be seen at the exit area of Shelikof Strait. Box shows the domain of the NPZ model.

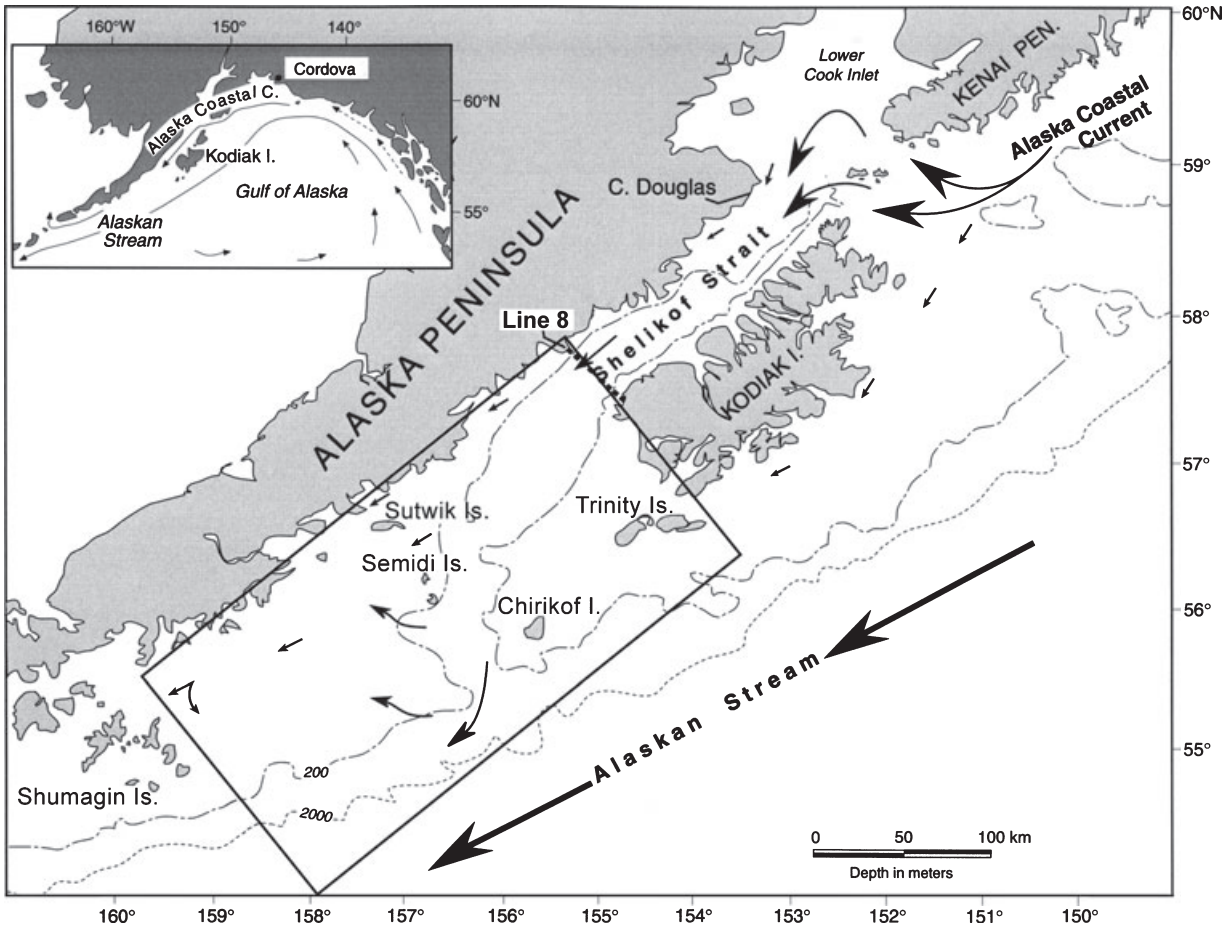

prediction of the effects of climate variability, and of different management strategies on this stock, and aid in understanding whether our management strategies are robust to climate change.

We previously used spatially explicit biophysical simulation models to examine recruitment dynamics of pollock in the western Gulf of Alaska (Hermann *et al.*, 1996, 2001; Hinckley *et al.*, 1996, 2001; Megrey and Hinckley, 2001). These models, which include a three-dimensional hydrodynamic model of the circulation in the area (Hermann and Stabeno, 1996; Stabeno and Hermann, 1996), and an individual-based model (IBM) of the early life stages of pollock (Hinckley *et al.*, 1996; Megrey and Hinckley, 2001) have been useful in testing hypotheses about recruitment processes, in integrating our knowledge, and in suggesting potentially useful directions for future research (see Werner *et al.*, 2001 for a review of other models).

In this paper we describe a three-dimensional nutrient–phytoplankton–zooplankton (NPZ) model that is integrated into our set of coupled models, and we use this model (in this study run separately from the pollock IBM, although it has also been used in a coupled mode, Hermann *et al.*, 2001) to examine possible effects of spatial and temporal patterns in the modeled availability of prey resources on recruitment of pollock in the western Gulf of Alaska. We examine the temporal and spatial evolution of the biological fields to assess hypotheses concerning the role of transport to the Shumagin Island nursery area, what may happen to larvae transported offshore or entrained in eddies, as well as how prey fields relate to recruitment.

This is one of the few three-dimensional NPZ models that have been developed specifically for the coastal regions of the Gulf of Alaska (Hermann *et al.*, 2001, in press; Hinckley *et al.*, in press). We hope that lessons learned in this research will aid in the development of other NPZ models for this region, especially for the coastal areas and those that are three-dimensional, as well as in the study of pollock recruitment.

METHODS

The physical model

The hydrodynamic model (described fully in Hermann and Stabeno, 1996) is a three-dimensional, prognostic, rigid-lid, eddy-resolving model of velocity and salinity fields in the northwestern Gulf of Alaska. The physical model domain encompasses the area from the east of Kodiak Island to the west of the Shumagin Islands (Fig. 1). The model solves the hydrostatic primitive hydrodynamic equations, with wind forcing distributed over the top 20 m of the water column, and buoyancy forcing (due to fresh-water runoff) along the coastline of Alaska. The wind field used to force the model is time-variable (12-hourly), and derived from Fleet Numerical Oceanographic Center modeled geostrophic winds. The monthly runoff time series of Royer (1982, Old Dominion University, Norfolk, VA, USA, unpublished data) was used. The model code was based on the semispectral primitive equation model (SPEM) of Haidvogel *et al.* (1991) modified for this region. The model employs a curvilinear-orthogonal horizontal coordinate system which follows the irregular coastline. Mean grid spacing in the area between Kodiak and the Shumagin Islands was 4 km. Beyond this region, the grid was expanded to broader spacing to allow for a large recirculation region (Hermann and Stabeno, 1996), which functions as a periodic boundary condition on the total alongshelf flux. Vertical structure was resolved using a depth-following ('sigma') coordinate system, with nine vertical levels.

Currents generated by the model have been compared with those measured by moored current meters and satellite-tracked drifting buoys (Stabeno and Hermann, 1996). The model reproduces dominant circulation features including the Alaska Coastal Current and the Alaskan Stream, with appropriate cross-shelf structure, vertical shear, and mean transport. Model floats tracked at 40 m (the mean depth of larval pollock abundance) using filtered model velocity fields compared favorably with observed drifter tracks at that depth (Stabeno and Hermann, 1996). Discrepancies between the circulation model and data were generally due to the formation of mesoscale eddies in the model at different times than those observed, although eddy statistics (e.g., rate of eddy formation, location) were similar for both. Further details of the model configuration and validation, including values of parameters, may be found in Stabeno *et al.* (1995), Hermann and Stabeno (1996), and Stabeno and Hermann (1996).

The biological model

This NPZ model was purpose-driven, i.e., it was developed to be part of a coupled model set used to study recruitment of walleye pollock, and its goal was to provide a dynamic prey source for larval walleye pollock. This goal resulted in certain simplifications in some areas, and added complexity in others. For example, nutrients (nitrate) and phytoplankton were each modeled as single compartments, whereas the *Pseudocalanus* spp. zooplankton compartment was stage-structured, to allow for consumption of different stages of nauplii and copepodites by larval pollock as they grow. A fuller discussion of potential advantages, disadvantages and consequences of this approach is presented in the Discussion section.

The NPZ model (Fig. 2) was modified from Frost's (1987, 1993) model to simulate processes in the coastal area (rather than the open ocean) and to model the specific food sources for young walleye pollock. The model was fully three-dimensional, and was run over a 20 × 20 subset of the circulation model grid. Horizontal resolution of the NPZ model was 20 km. Biological boundary conditions at the upstream (northern) end of the NPZ model grid were derived by running the model in one-dimensional mode (no advection or horizontal diffusion) at each upstream boundary grid point. Boundary values were advected into the interior, driven by the velocity field. At the downstream boundary and along the coastal and ocean boundaries, a zero horizontal gradient was imposed for all biological variables.

The water column was 100 m deep or the depth of the ocean bottom, whichever was less. The model contained 100 explicit vertical depth bins; however, overlying this structure were three main vertical regions, similar to Frost (1993), i.e., a homogeneous mixed layer (which varied daily in depth), a vertically stratified layer extending to 100 m depth or to 1 m above the bottom, and a lower layer, where the values of the state variables were assumed to be constant (this was the bottom boundary condition for the stratified layer). Values of state variables in the mixed layer were blended at each time step, but the depth-dependent non-conservative terms (e.g., light limitation on growth) were calculated separately at each of the 100 vertical depth bins.

Exchange between the mixed layer and the stratified layers below, and between each stratified layer was assumed to be a result of turbulent diffusion and the change in depth of the mixed layer (where 'mixed' denotes that vertical mixing is infinitely fast). Background eddy diffusivity in the stratified layer (k_v) was

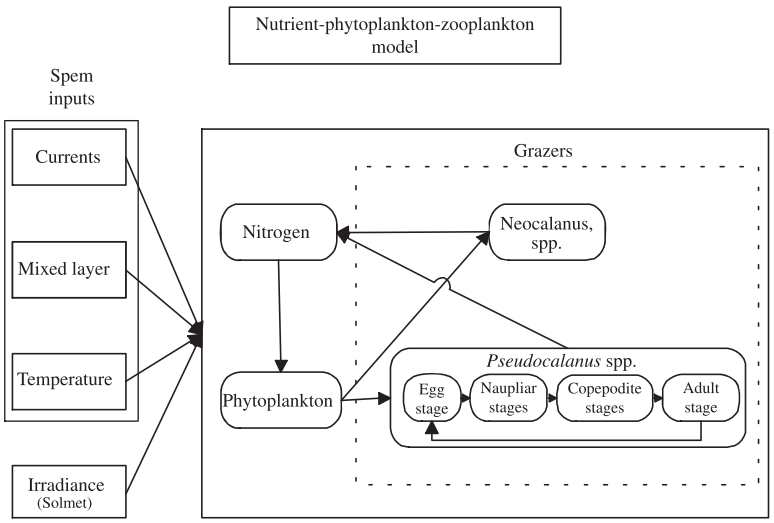

Figure 2. Flow chart of the NPZ model. Physical forcing inputs are to the left. 'SPEM' refers to the Semispectral Primitive Equation Model, i.e., the hydrodynamic model.

assumed to be vertically isotropic and was set to the same value used by the circulation model (Hermann and Stabeno, 1996, Appendix 3a,b). The tendency terms due to mixing were therefore:

$$\text{Mixing} = \frac{k_v}{\text{MLD}}(X_{\text{MLD}+1} - X_{\text{MLD}}) \quad \text{(Mixed layer)} \tag{1}$$

$$\text{Mixing} = k_v(X_{z-1} + X_{z+1} - 2X_z) \quad \text{(Stratified layer)} \tag{2}$$

where X is concentration of state variable (m^{-3}), and the rest of the parameters, notation and terms are defined in Appendices 1 and 3a,b.

The NPZ model simulated nutrients (nitrate), phytoplankton, a large herbivore grazer parameterized as *Neocalanus* spp. and 13 stages (eggs, naupliar and copepodite) of *Pseudocalanus* spp., a major constituent of the diet of young pollock. Because this model was designed to reproduce feeding conditions for young pollock, complexity was confined to the most important elements, i.e., to the stage-structuring of *Pseudocalanus* spp. Young pollock eat different stages of *Pseudocalanus* spp. as the fish grow (Kendall and Nakatani, 1992; Napp *et al.*, 1996). The rest of the model was reduced to the level of complexity necessary to reproduce ecosystem dynamics that affect pollock prey.

Carbon (mg m^{-3}) was the currency of the model, except for nutrients, which were followed in units of nitrogen (mmol N m^{-3}). The Redfield ratio (Redfield *et al.*, 1963) was used to convert carbon to nitrogen. The time step of the model was 0.1 day.

State variable and subscript notation are explained in Appendix 1. Specific equations for each model component and for processes are presented and explained in Appendix 2. Parameter values for the NPZ model are shown in Appendix 3a,b. General model formulations are shown below.

Nutrients:

$$\frac{dN}{dt} = -\text{Photosynthesis} + \text{Excretion} + \text{Mixing} \tag{3}$$

Phytoplankton:

$$\frac{dP}{dt} = \text{Photosynthesis} - \text{Grazing} + \text{Mixing} \tag{4}$$

Neocalanus spp.:

$$\frac{dH_1}{dt} = \text{Growth} - \text{Mortality} + \text{Mixing} \tag{5}$$

Pseudocalanus spp. eggs:

$$\frac{dH_2}{dt} = \text{Egg production} - \text{Transfer to } H_3 - \text{Mortality} + \text{Mixing} \tag{6}$$

Pseudocalanus spp. nonfeeding stages N1 and N2 (i = 3, 4):

$$\frac{dH_i}{dt} = \text{Transfer from } H_{i-1} - \text{Mortality} - \text{Transfer to } H_{i+1} + \text{Mixing} \tag{7}$$

Pseudocalanus spp. feeding stages N3 – C6 (i = 5,...,14):

$$\frac{dH_i}{dt} = \text{Transfer from } H_{i-1} + \text{Growth} - \text{Mortality} - \text{Transfer to } H_{i+1} + \text{Mixing} \tag{8}$$

Microzooplankton were not included in this NPZ model, as there were few data on their abundance and

rates of grazing or production in the Shelikof Strait area. Also, although the effect of iron limitation on phytoplankton growth is well known in the open Gulf of Alaska basin, and perhaps on the shelf in some regions (Strom *et al.*, 2007), it was not included in this model. We were modeling the coastal region only, in an area (Shelikof Strait to Shumagin Island region) where the onshore transport of iron-poor water is not likely to be important to the production of food for young pollock. Phytoplankton growth was therefore limited only by light and nutrient availability.

The biological model was run from day of year (DOY) 70 to DOY 165 using an explicit leapfrog scheme for the time stepping (0.1 day) with an Asselin (1972) time filter to damp out the computational mode (i.e., high frequency numerical artifacts).

Parameter optimization for the biological model

Some of the least known parameters in the NPZ model were optimized, i.e., tuned to fit a portion of the data collected in Shelikof Strait, using a one-dimensional version of the model [the full three-dimensional model took too long (154 h) to run for optimization purposes]. Data available for model optimization were sparse. Most of the observations were from stations on a transect line across the exit region of Shelikof Strait (Line 8, Fig. 1); data were available for all state variables at this location. For model optimization, data from 1987 were averaged across stations on Line 8.

For the optimization, a specified number of random sets ($N = 1000$) of model input parameters were drawn from a triangular distribution using the Latin Hypercube technique (McKay *et al.*, 1979; Megrey and Hinckley, 2001). Then, each parameter set was used by a single model run. Each model run generated a set of output variables which were then averaged over depth and Line 8. Acceptable sets of parameters were defined as those that resulted in model output variables which fell within the range of observed data. Of the acceptable sets of parameters, the best fitting was determined visually, as the data were so sparse.

Biophysical model coupling

The physical and biological models were run sequentially, due to (i) the longer time needed to run the physical model, and (ii) the need for multiple runs of the biological model for each physical model year. The circulation model was run with forcing appropriate to the particular year. The output was stored as low-pass filtered daily velocities, temperatures and salinities, for use by the NPZ model (Hermann *et al.*, 2001). The NPZ model was run on a coarser grid than the physical model, as discussed earlier. Some of the finest resolution features of the circulation were lost when using this method. Therefore we did not attempt to examine features smaller than mesoscale eddies in this set of model experiments. However, eddies are relatively well represented by the physical model (which has a horizontal scale of ~4 km), as in the Shelikof region these features average 30–40 km in diameter (Bograd *et al.*, 1994; Stabeno *et al.*, 2004). Although the NPZ model grid spacing is somewhat coarse to resolve these features with much precision, they are still easily discernible in model output.

Given the use of multiple grids, we needed to project the circulation field onto the NPZ grid in a consistent manner. The circulation model produces information regarding both the depth-averaged velocity field (the barotropic component) and its vertical structure (the baroclinic component). A naïve interpolation of the raw barotropic plus baroclinic velocities from the three-dimensional circulation model grid onto the different spatial grid of the NPZ model in fact led to substantial convergence errors, which in turn led to spurious vertical velocities with severe biological consequences (e.g., inappropriate injection of nutrients). A less problematic and more cautious approach was therefore taken, by distributing the depth-averaged velocity into the top 100 m of the water column (or the entirety of the water column for shallower bathymetry). This retained the basic horizontal advection of NPZ components in the upper layers, and conformed to the basic vertical structure of the currents (strongest currents in the upper water column, weakest at depth), at the expense of detailed information about vertical shear. Depth-dependent vertical velocities at each location were calculated from the vertical integral of the horizontal convergence of this simplified field. While this is clearly a broad simplification of the true three-dimensional velocity field, the approach nonetheless retains many of the important physical phenomena, such as vertical advection at the edges of mesoscale eddies, known to have a significant impact on local production.

Simulations and analysis

The runs of the model analyzed in this study were: 1978, 1987, 1988, 1989, 1991 and 1994. These years span a wide range of system conditions (winds, runoff), and recruitment success of walleye pollock (Table 1; see also Hermann *et al.*, 1996). Months were classified as weak, moderate or strong based on levels of runoff or downstream (southwestward in Shelikof Strait) wind stress. The years analyzed may be considered natural experiments involving two fundamentally different 'treatments': runoff and winds. Conditions for

the simulated years include: a year with average runoff and strong winds which resulted in strong recruitment (1978), a wet year with average–strong winds which resulted in weak recruitment (1987), a wet, windy year with strong recruitment (1988), a dry, moderately calm year with weak–moderate recruitment (1989), and two moderate runoff years with weak to moderate winds and weak to fairly weak recruitment (1991 and 1994). These years were analyzed for spatial and temporal patterns in production of pollock prey.

Model outputs for nauplii were compared to data from NOAA's Fisheries Oceanography Coordinated Investigations (FOCI) program (separate from the data used for the optimization). Data used were from 3 years (1986, 1987 and 1989) at Line 8. Because the data were sparse, available data were combined, and output from the model was compared to the depth- and station-averaged data (over Line 8). We also compared model outputs (chlorophyll) to satellite chlorophyll images to see whether the spatial patterns identified in the model were visible. Satellite image files were downloaded from the Ocean Color Browse directory at http://oceancolor.gsfc.nasa.gov/cgi/browse.pl and processed with SeaDAS, (http://oceancolor.gsfc.nasa.gov/seadas/). No satellite images were available for the modeled years, so we searched for similar patterns from other years (1998–2008). Files from 1998 to 2003 are SeaWiFS files, and files from 2004 to 2008 are Aqua MODIS files.

Table 1. Interannual variability in runoff, winds and recruitment, derived from Hermann *et al.* (1996). Recruitment estimates from Dorn *et al.* (2007).

Year	Month	Runoff	Winds	Abundance of age-2 recruits (millions)
1978	March	Weak	Moderate	3485
	April	Moderate	Weak	
	May	Strong	Moderate	
1987	March	Strong	Strong	368
	April	Moderate	Moderate	
	May	Strong	Moderate	
1988	March	Moderate	Strong	1688
	April	Strong	Strong	
	May	Moderate	Moderate	
1989	March	Weak	Moderate	1080
	April	Weak	Moderate	
	May	Moderate	Weak	
1991	March	Weak	Weak	252
	April	Moderate	Moderate	
	May	Strong	Moderate	
1994	March	Weak	Moderate	829
	April	Moderate	Weak	
	May	Strong	Moderate	

RESULTS

Seasonal variability

The modeled sum of *Pseudocalanus* spp. naupliar stages is shown, for all years, in Fig. 3. In all years except 1989, naupliar concentrations reached the threshold level for larval pollock growth and survival of 20 000 m^{-3} (Theilacker *et al.*, 1996) by about DOY 110–115. In 1989, this level was not reached until after DOY 140. The number of nauplii on DOY 120 was of interest. If eggs are spawned on DOY 95 (Kendall *et al.*, 1996), spend 2 weeks in the egg stage (Blood *et al.*, 1994), and then 5–7 days in the yolk sac stage (Bailey and Stehr, 1986), they would be ready to feed at about this time. The highest modeled

Figure 3. Modeled *Pseudocalanus* spp. concentrations (sum of naupliar stages) (n m^{-3}) averaged over the mixed layer for all years at Line 8. *Observed values from Line 8 in 1986, 1987 and 1989 (averaged over year, depth and station). The model was optimized for 1987, so the differences in the simulation were due to physical forcing. Note that the fits to the data are reasonable except for 1989.

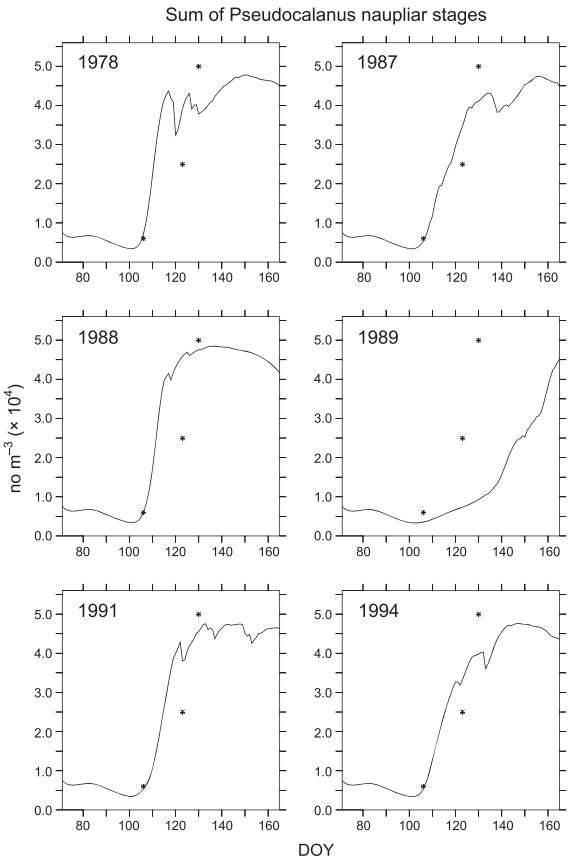

concentrations of nauplii on DOY 120 were seen in 1978, 1987, 1988 and 1991, with somewhat smaller numbers in 1994, and the lowest concentrations in 1989. Note that the fit to the averaged data (from 1986, 1987 and 1989) was quite good for all years except 1989. The model was only tuned to 1987, so the interannual differences in naupliar numbers is due to differences in physical forcing for each year. In 1989, there were two data points showing an earlier increase in nauplii.

Horizontal variability in prey resources

The interannual variability in the modeled spatial (horizontal) distribution of prey for larval pollock, here represented by the sum of the naupliar stages of *Pseudocalanus* spp., was of special interest. We were able to identify several phenomena in these distributions, and we discuss these separately, and illustrate them with examples from the model output.

Regions of low abundance of nauplii

There were two areas that had consistently lower concentrations of *Pseudocalanus* spp. nauplii after the spring bloom had occurred: the southwest shelf between the Semidi Islands and the Shumagin Islands, and the Trinity Banks area just southwest of Kodiak Island (Fig. 4, using 1994 as an example). The Trinity Banks area is not one where larval pollock are often seen, so this is not discussed further. The Semidi–Shumagin area is, however, an important nursery area, as mentioned previously.

For all years except 1988, naupliar concentrations were below 20 000 nauplii m^{-3} in the Semidi-Shumagin area through DOY131 (mid-May). By DOY 141 (mid-late May), in 1987, 1989 and 1994 and until DOY 151 (early June) in 1987 and 1989, average naupliar abundances in this region still had not reached 20 000. In 1978 and 1991, the region of low abundance was smaller and more compressed against the coast. By the end of the model run (mid-June), naupliar concentrations in this region remained low (<25 000), especially in 1987 and 1989.

Figure 5 shows modeled chlorophyll fields for 6 days in 1994. Note that the low abundance area was visible for chlorophyll, as well as for nauplii (Fig. 4). Figure 6 shows some days/years of composite satellite images for which this gap area was also visible. It was not quite as consistently present in the satellite images as in the model output (for example, see Fig. 10), but could often be seen. One feature of note in the satellite images was a large region of high chlorophyll often seen in and around the Shumagin Islands. At times, this region appeared to be the source of chlorophyll intruding into the region to the east. This high abundance area was not seen in the model output, as it is, for the most part, outside (to the west of) our NPZ model domain.

High abundance areas

Early in the year (mid-April), there were a few patches of slightly elevated concentrations in small regions, such as near the Trinity Islands and the exit region of Shelikof Strait, and along the Alaska Peninsula. By early May, a region of higher abundance stretched down the sea valley from Line 8 to the sea valley exit region in 1978, 1991 and 1994. Some very high concentrations (>45 000) were seen in small patches at Line 8 on the Alaska Peninsula side in early May in 1987, 1988, 1991 and 1994. By mid-May, areas of higher than background concentrations were very patchy, but generally followed the flow down the sea valley.

Regions of highest naupliar concentrations generally followed the flow (as indicated by the stream function, Fig. 7). In years with few eddies (1978, 1989, 1991 and 1994), the high concentrations were evenly spread down the sea valley, whereas in years rich with meanders and eddies (1987 and 1988), high concentrations were located in and around cyclonic eddies, and between eddy dipoles (see next section).

In many years, starting in early May in 1978 and in mid-May in 1988, a region of high naupliar concentrations occurred in the model extending down the sea valley and out along the shelf break west of the Shelikof Strait exit region (Figs 7 and 8). This region of high abundance extended onto the shelf (inshore of the 200 m contour) east of the Shumagin Islands in some years.

Figure 9 shows that the pattern of high abundance following the flow was visible in the modeled chlorophyll output as well as the nauplii. Figure 10 indicates that this feature was also visible in the composite chlorophyll images, although of course we don't know the details of the flow in these images. Note, however, that there were sometimes high abundances of chlorophyll along the shelf break to the east of the sea valley, to the south and southeast of Kodiak Island. This feature was not seen in the model output. Also not seen in the model output were areas of high chlorophyll biomass seen very close to the coast in Fig. 10.

Eddies

In the NPZ model output, there often was a general pattern of higher abundances of naupliar stages in and around cyclonic (counterclockwise) eddies, and lower abundances in the anticyclonic eddies (Fig. 11). Sometimes areas of higher abundances are seen around

Figure 4. Contours of the sum of the naupliar stages (n m^{-3}) in 1994. Black lines are depth contours (m). t is Day of Year. Note that the region between the Semidi and Shumagin Islands is relatively poorer in nauplii than the exit region of Shelikof Strait and the sea valley for most of the model run.

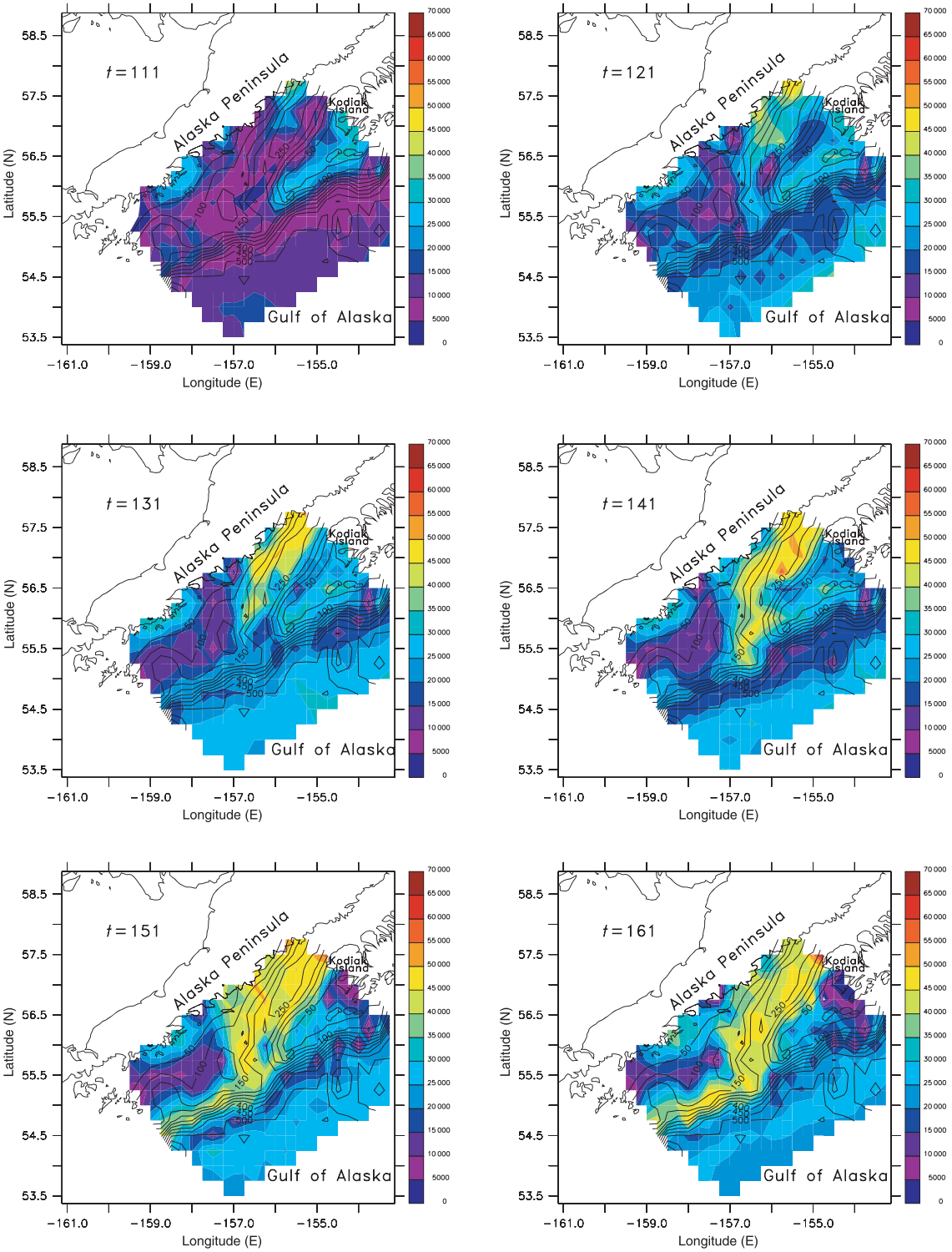

Figure 5. Contours of phytoplankton chlorophyll (mg m^{-3}) in 1994. Black lines are depth contours (m). *t* is Day of Year. Note that the region between the Semidi and Shumagin Islands has relatively less phytoplankton than the exit region of Shelikof Strait and the sea valley for most of the model run, as is true for nauplii.

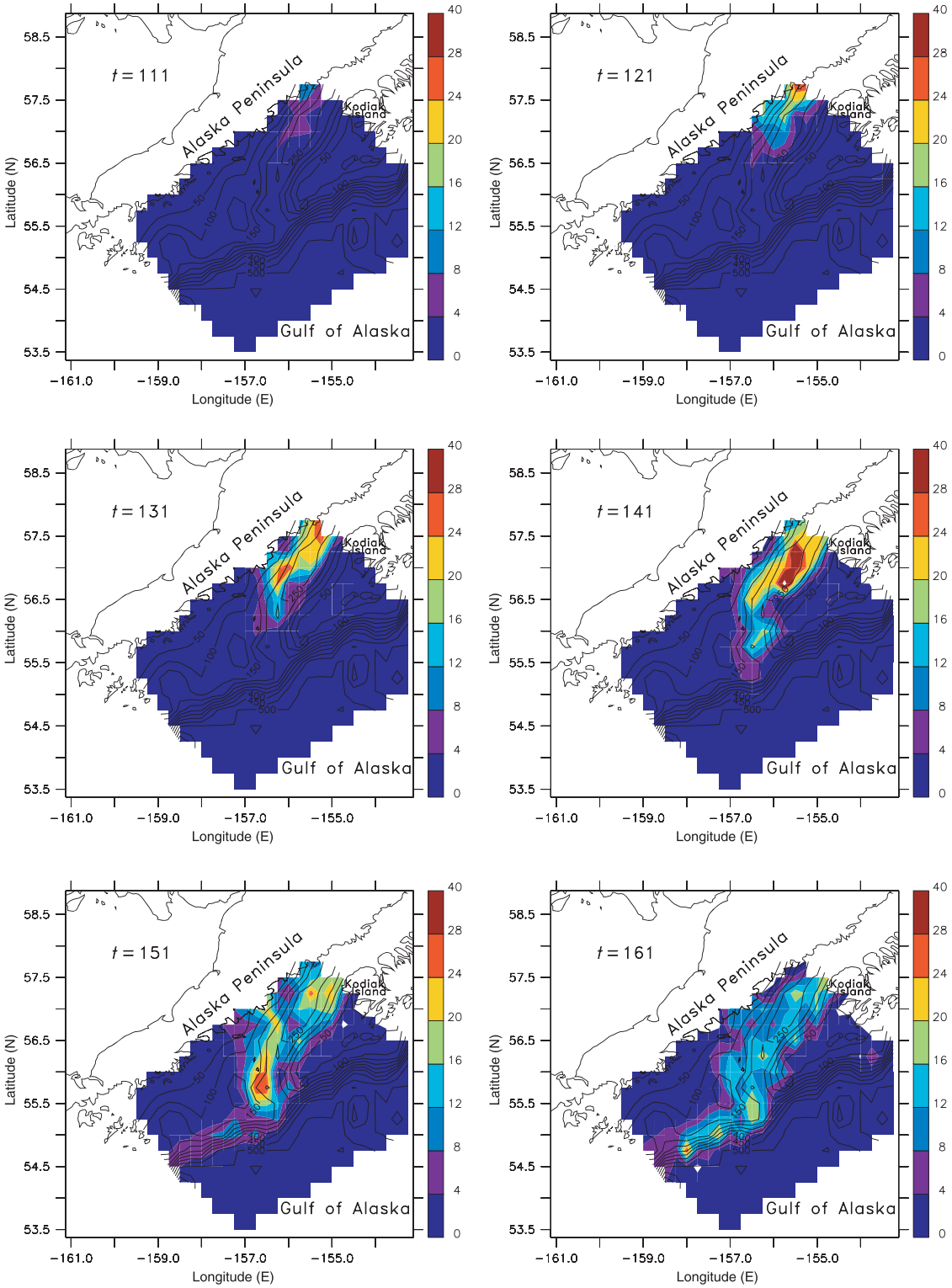

Figure 6. Five-day composite satellite chlorophyll images for various years and days, showing low abundance region between the Semidi Islands (top left, red arrow) and the Shumagin Islands (top right, yellow arrow).

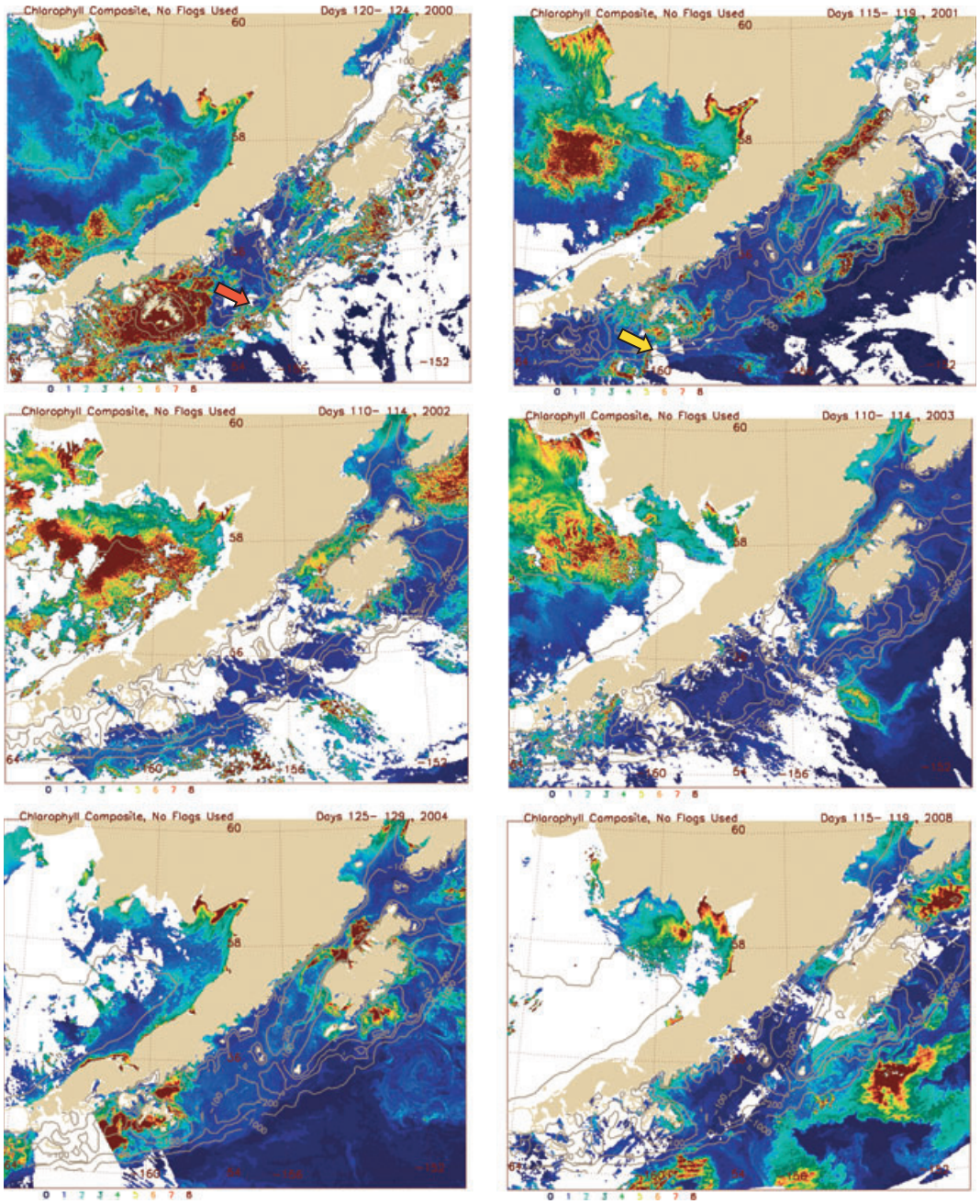

the edges of anticyclonic eddies and between eddy pairs. One mechanism of enhanced production in cyclonic eddies could be via shallowing of the mixed layer and nutrient resupply. We examined the distribution of mixed layer depth (MLD) and noted that MLD was indeed shallower in the cyclonic eddies, and deeper in the anticyclonic eddies (Fig. 12). Standing stocks of phytoplankton also were higher in the center of the cyclonic eddies, relative to the anticyclonic eddies (Fig. 13), due to enhanced nutrients.

This feature of modeled naupliar abundance being found in cyclonic eddies was not generally visible in satellite chlorophyll images, due to a lack of information about flow directions, as well as a lack of sequential images (due to clouds) necessary to identify eddies clearly.

Figure 7. Contour lines of the sum of the naupliar stages of *Pseudocalanus* spp. of DOY 121 in 1988. Contour units are $n\ m^{-3}$. Black solid lines are depth contours. Red lines are streamfunctions. Positive values of the streamfunction are solid and negative values are dashed. Note how regions of high abundances follow the streamfunction (flow) lines.

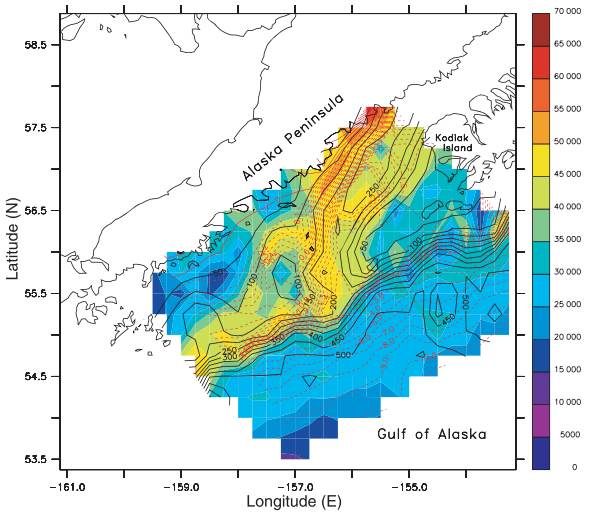

Figure 8. Contour lines of the sum of the naupliar stages of *Pseudocalanus* spp. of DOY 141 in 1991. Black solid lines are depth contours. Red lines are streamfunctions. Note the extension of the region of high abundance out of the Shelikof sea valley along the continental shelf to the west.

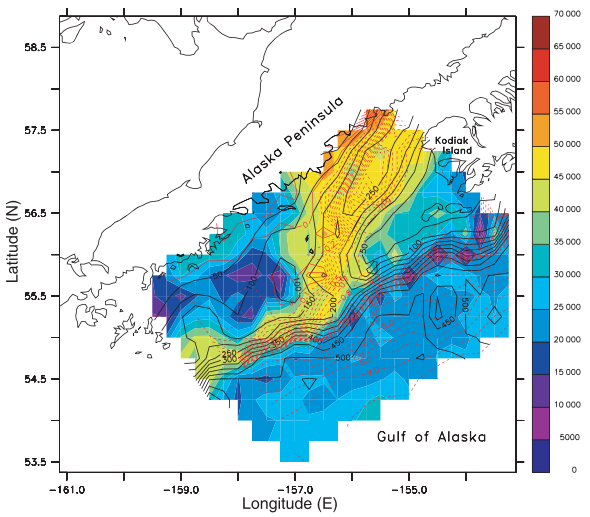

DISCUSSION

Spatially explicit biophysical models can be powerful tools for examining hypotheses about the early life history of fish and linkages between these stages, their prey and recruitment (see Werner *et al.*, 2001 for a review). Earlier models of this type have coupled hydrodynamic models with individual-based models (IBMs) of fish early life history. The prey for these early stages, if included at all, has usually been static. Werner *et al.* (2001) state, however, that '…to date the population dynamics of prey (e.g., copepods) have been studied separately from those of the predators (e.g., fish larvae)'. This is a reason why further examination of some theoretical questions related to recruitment, such as Cushing's (1972, 1974) match–mismatch hypothesis, have seldom been investigated with this type of modeling. This work addresses the deficiency noted by Werner *et al.* (2001); our coupled models now include a spatially and temporally explicit model of prey production. In the present manuscript, we present results from a three-dimensional NPZ model designed to simulate the prey of larval walleye pollock in the western Gulf of Alaska, and attempt to relate prey conditions to recruitment variability in this species.

Models are simplifications of real ecosystems. As such the results reflect the sensitivity of the model to assumptions, the structure of, and functions in, the model. Our focus was on the production of prey (*Pseudocalanus* spp.) for larval pollock, and due to this and the state of physical model development for the region at the time this work was started, our model had several structural simplifications that should be emphasized. For example, data from a single year's temperature cycle were used in the biological model (Appendix 4). Although the spatial pattern of temperature varies by year for the 6 model years where the temperature field is advected and diffused, the effect of an interannually invariant temperature is unknown. There are processes in the model, e.g., the doubling rate of phytoplankton, egg production rate and the hatch rate of *Pseudocalanus* spp. eggs, and stage duration of *Pseudocalanus* which were dependent on temperature. With this model we could examine spatially dependent temperature-related patterns and seasonal/temporal temperature-related patterns; however, we could not examine the effect of exceptionally warm or cold years.

Also, the NPZ model, and especially the bloom dynamics and hence the *Pseudocalanus* production in the model, is extremely sensitive to variations in MLD. The version of the hydrodynamic model used in these simulations (SPEM) had no explicit mixed layer. The approximation we employed, using the distribution of density over depth, was less adequate than a physical model that contains an explicit mixed layer. Wind events can affect bloom dynamics by changing the depth of the mixed layer, and therefore events seen in the data will not always be replicated by the model. The newer hydrodynamic model (ROMS; Haidvogel *et al.*, 2000, 2008) which has been adapted

Figure 9. Contours of modeled phytoplankton chlorophyll (mg m^{-3}) on (top left) DOY 121, 1988, (top right) DOY 141, 1991, and (bottom) DOY 151, 1991. Black solid lines are depth contours. Red lines are streamfunctions. Note that regions of high abundance of chlorophyll follow the flow, as well as the extension of the region of high abundance out of the Shelikof sea valley along the continental shelf to the west.

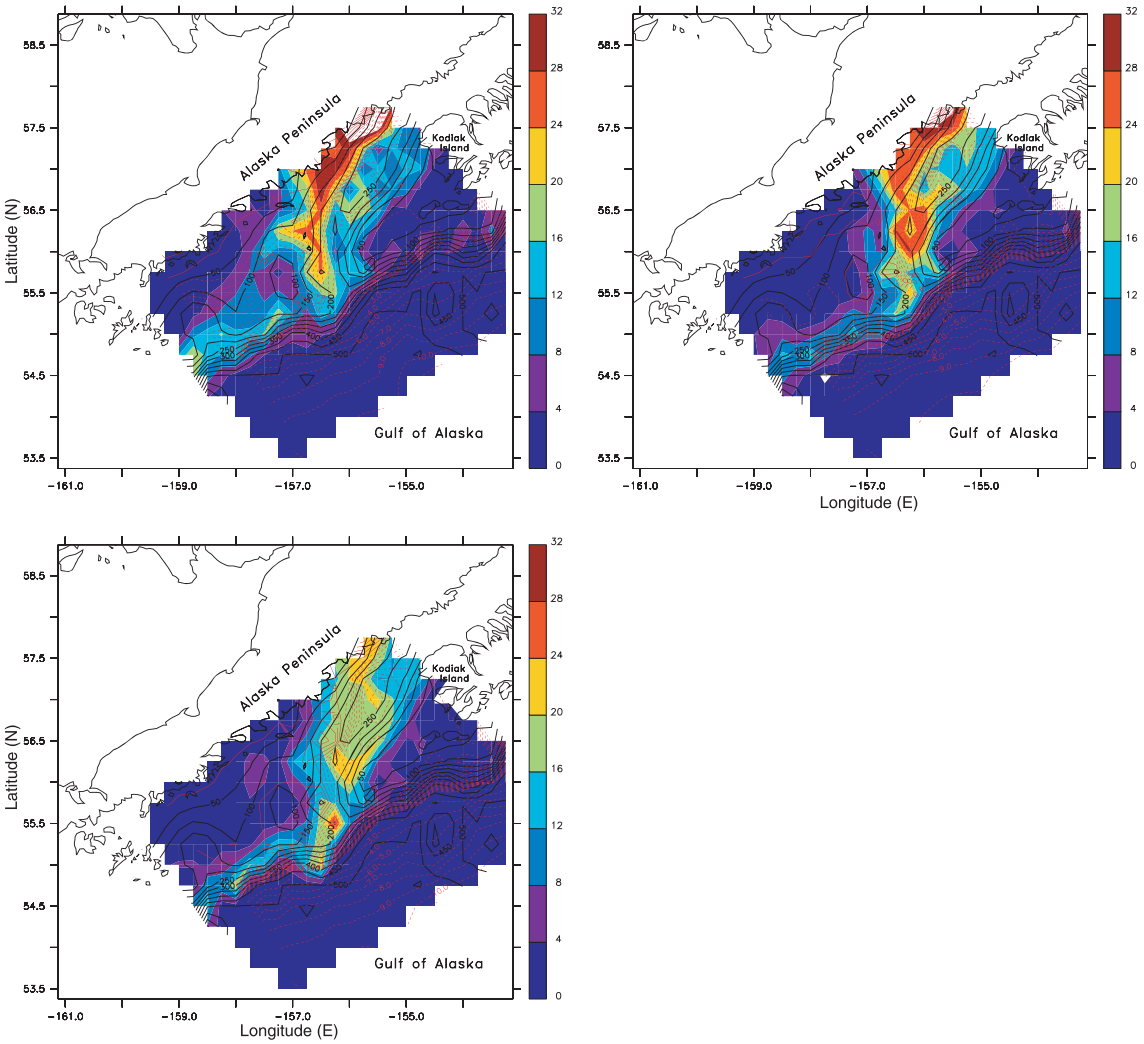

for this region and will be used with these biological models in the future, includes explicit mixed layer dynamics and realistic temperature fields.

If these newer physical models run faster than the SPEM model, it may also be possible to run the NPZ model online, i.e., integrated with the physics. This will avoid many of the problems faced when running the model offline, such as lack of resolution and inaccuracies due to using different grids.

Our model also lacked microzooplankton grazers. The absence of microzooplankton certainly affected modeled phytoplankton dynamics. Phytoplankton blooms in this region are generally shorter in duration than we saw in this model, most likely due to our lack of a realistic loss (grazing) term. In general, chlorophyll biomass before DOY 110 was adequately represented by the model, but diverged thereafter. Given the low phytoplankton concentrations assumed necessary to reach maximum *Pseudocalanus* egg production, and the good agreement between data and the model for *Pseudocalanus* naupliar concentrations, we believe that the initial production of *Pseudocalanus* nauplii was not greatly affected by our simplistic modeling of the phytoplankton component or competition with microzooplankton for food.

Iron limitation of phytoplankton production is well known for the open subarctic Pacific (Martin *et al.*, 1989; Strom *et al.*, 2000; Harrison *et al.*, 2004). Recent evidence indicates that it may occur at certain times on the Gulf of Alaska shelf in areas

Figure 10. Five-day composite satellite chlorophyll images for (top left) DOY 120–124, 2001, (top right) DOY 125–129, 2001, (middle) DOY 120–134, 2001, (bottom left) DOY 145–149, 2004, and (bottom right) DOY 150–154, 2004. Note how regions of high chlorophyll extend down the Shelikof sea valley and along the shelf break to the west. Note also (top right and middle) area of high production along the shelf break to the east, south and southeast of Kodiak Island, as well as a consistently high biomass of chlorophyll near the coast.

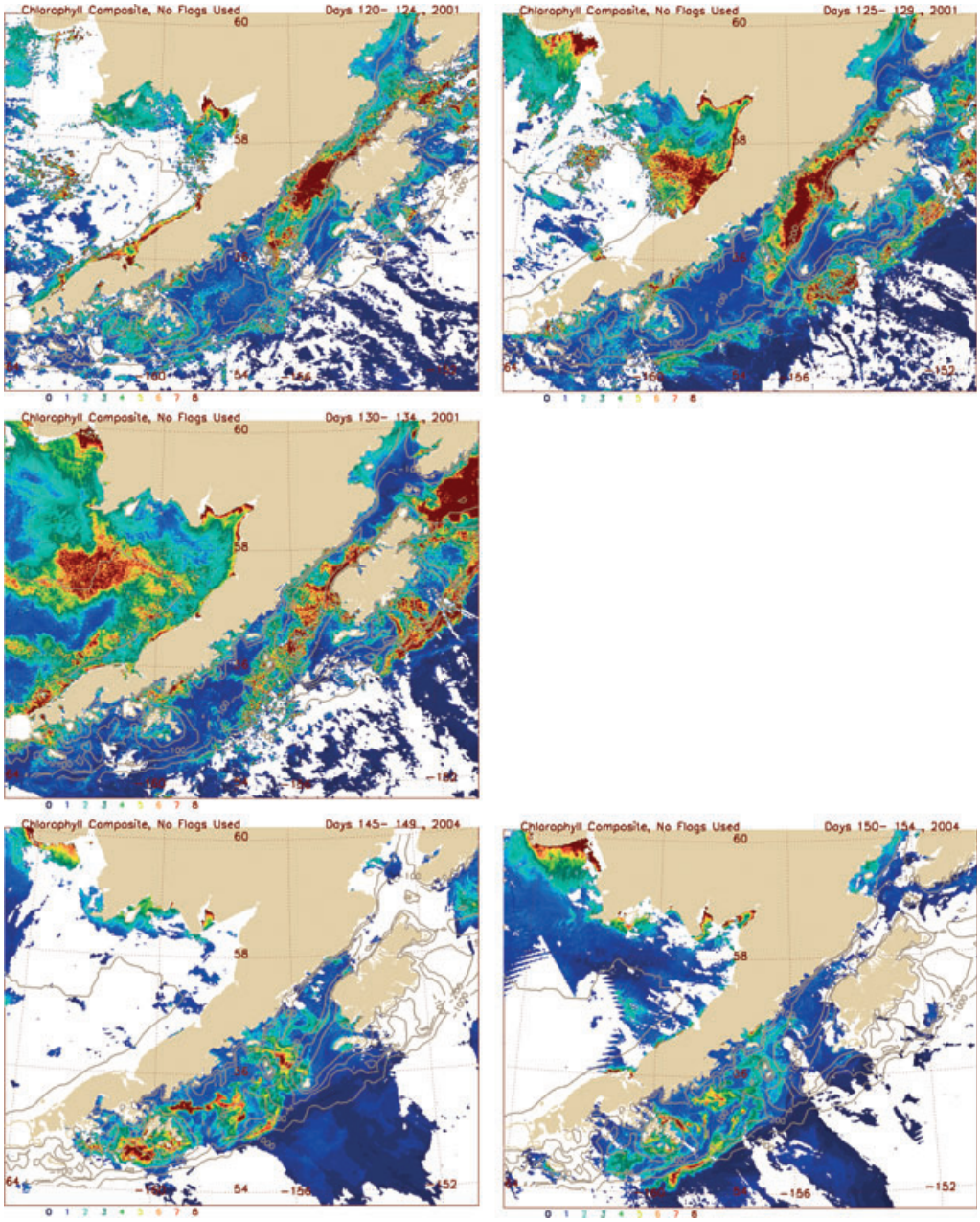

where there are episodic intrusions of open ocean waters (Strom *et al.*, 2007). Our model considered light and macronutrient (nitrogen) limitation of phytoplankton growth only. In our judgement, the lack of iron should not significantly affect dynamics in the study region, where the Alaska Coastal Current water is thought to control the biological dynamics (Kendall *et al.*, 1996; Stabeno *et al.*, 2004).

The lack of adequate data to corroborate or refute the model was a problem. For example, much of the copepod naupliar abundance data available in the western Gulf of Alaska region came from a single time-series transect location (Line 8) in Shelikof

Figure 11. Contours of the sum of the naupliar stages (n m^{-3}) on DOY 161 in 1994. Black solid lines are depth contours. Red lines are streamfunctions. Note that naupliar numbers are higher in cyclonic eddies (closed, dotted red lines), than in anticyclonic eddy (closed, solid red lines).

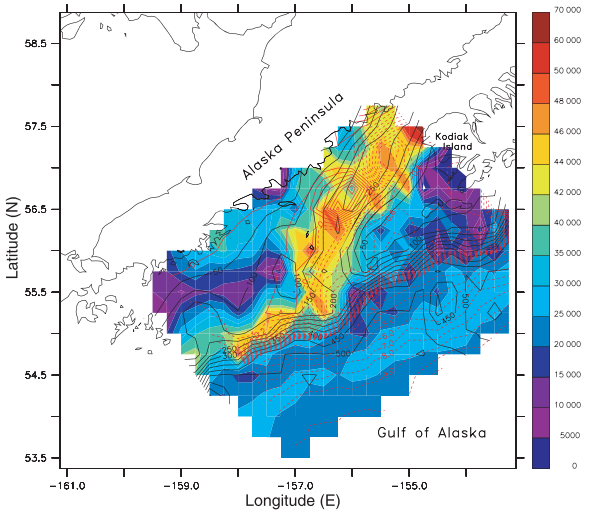

Figure 12. Contours of mixed layer depth (MLD, m) on DOY 161 in 1994. Black solid lines are depth contours. Red lines are streamfunctions. Note that MLD is shallower in the cyclonic eddy (closed, dotted red lines) than in the anticyclonic eddy (closed, solid red lines).

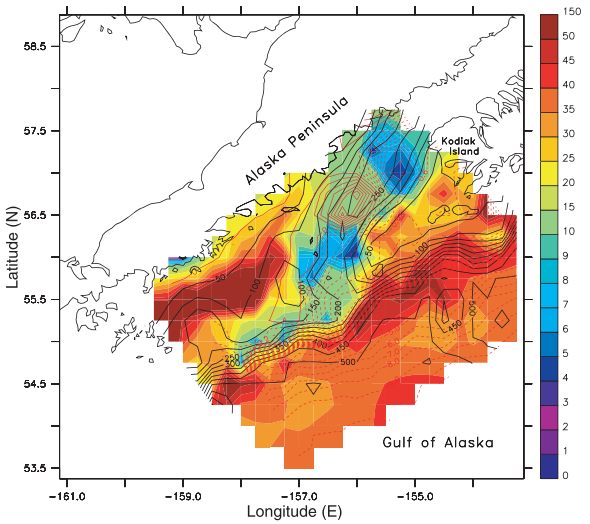

Strait. We had virtually no data to compare with the rest of the model domain. This is likely to continue to be a problem, due to the large spatial domain (~65 000 km^2) and expense of collecting and analyzing these data.

Despite these issues, simulations of the temporal and spatial dynamics of copepod nauplii, the main prey resource of young pollock (Kendall and Nakatani, 1992; Napp *et al.*, 2005), resulted in some interesting observations. One was the finding that the coastal area between the Semidi Islands and the Shumagin Islands showed consistently lower levels of nauplii, especially early in the year. It would not appear to be advantageous for young pollock to be transported to this area early in the year (before mid-late May). The early hypothesis concerning the necessity of alongshore transport to the Shumagin Island nursery area, and possible negative effects of transport offshore or into the Alaska Stream may require modification. This model result, showing this region of low abundance early in the year, suggests that retention in the Shelikof sea valley early in the spring, instead of fast transport to the nursery area, would be advantageous. This provides a testable hypothesis; that recruitment success is increased if young pollock are not transported to the nursery area too early in the year.

Figure 13. Contours of phytoplankton biomass (mg chlorophyll m^{-3}) on DOY 161 in 1994. Black solid lines are depth contours. Red lines are streamfunctions. Note that chlorophyll levels are higher in the cyclonic eddy (closed, dotted red lines) than in the anticyclonic eddy (closed, solid red lines).

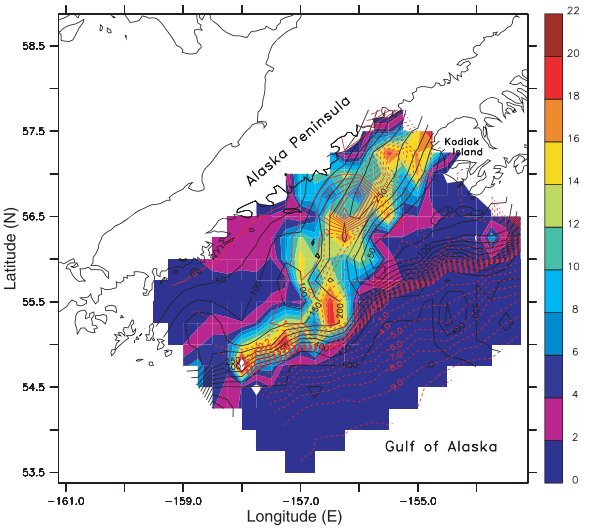

Also, this modeling suggested that when larvae are carried out of the Shelikof sea valley along the shelf break, prey may be advected in the same water parcels as larvae (see IBM experiments described in Hermann *et al.*, 1996). This transport was seen in the NPZ model year 1988, and to a somewhat lesser extent in 1978 and 1991. Both 1978 and 1988 were exceptional year classes (Megrey *et al.*, 1995). Part of the original hypothesis mentioned above was that larvae transported away from the sea valley and coastal areas were

likely to starve. The larvae that go offshore may not, however, be subject to food deprivation if prey are carried with them in the same water parcels and they are unable to deplete their prey during transit. These parcels of water may be carried back onto the shelf into the nursery areas (e.g., east of the Shumagin Islands); however, they may also be carried too far downstream to get to the nursery areas or to recruit back to Shelikof Strait, unless behavioral mechanisms, such as onshore swimming of the juvenile pollock, exist.

We were also able to examine the hypothesis that entrainment in eddies may be beneficial to larvae (as hypothesized by Kendall *et al.*, 1996), even though the NPZ model only coarsely resolved these eddies. In this modeling study, naupliar concentrations were often higher in and around cyclonic eddies than in anticyclonic eddies. This is an emergent property of the model relationship between mixed layer, phytoplankton growth and *Pseudocalanus* production. Several studies have found higher larval pollock numbers in eddies (Canino *et al.*, 1991; Bograd *et al.*, 1994; Stabeno *et al.*, 1996); however, only one of these (Canino *et al.*, 1991) also measured prey availability. In that study, prey was found to be higher in the eddy, which was cyclonic. The number of nauplii in larval stomachs and the larval condition (as measured by RNA/DNA ratios) were also higher in the cyclonic eddy (Canino *et al.*, 1991).

There are several potential consequences of retention in eddies. One is that, since eddies are translated downstream more slowly than average transport rates, retention in eddies means that larvae do not get transported too quickly to a possibly prey-deplete region to the west of the sea valley. Another possible consequence is higher growth rates (and lessened mortality rates) due to higher prey levels in cyclonic eddies. Cyclonic eddies are characterized by stratification at shallower depths than the surrounding waters, whereas anticyclonic eddies show a deeper mixed layer. Shelikof Strait is not a nutrient limited region until after the spring bloom, when nutrient levels in the surface layer can drop to zero (Incze and Ainaire, 1994; Napp *et al.*, 1996). Nutrients may be limiting later in the spring near the surface in anticyclonic eddies due to depression of the nutricline, which may decrease new and total production if the mixed layer is deeper than the compensation depth, eventually limiting production of nauplii. Higher phytoplankton production has also been seen in cyclonic eddies in the Kuroshio Frontal region (Kimura *et al.*, 1997), in wind-driven cyclonic eddies in the lee of the Hawaiian Islands (Bibby *et al.*, 2008; Mahaffey *et al.*, 2008) and in cyclonic eddies off California (Hayward and Mantyla, 1990).

Whatever the mechanism, it seems that, under certain circumstances, larvae entrained in cyclonic eddies may do better than those in surrounding waters or in anticyclonic eddies. We also saw (in the model results) shallower mixed layers and higher concentrations of phytoplankton in the cyclonic eddies than in the anticyclonic eddies. However, anticyclonic eddies are twice as common in the Shelikof Strait and sea valley as cyclonic eddies (Bograd *et al.*, 1994, P. Stabeno, Pacific Marine Environmental Laboratory, Seattle, WA, USA, pers. comm.), possibly because anticyclonic eddies may be more stable, so the overall implications of this model finding for recruitment are unclear.

A question of interest about the production in the Shelikof Strait region, especially as it provides prey for larval pollock, is how much of this production is local and how much of it is advected – either in from north of the region or within the region. One cannot, of course, look at modeled naupliar evolution/distribution farther northward than the model boundary at Line 8; however, one can examine this question of local/advective production within the model domain. What we have seen in movies of naupliar distribution, which obviously cannot be included here, is that isolated areas of local production arise early in different coastal and downstream areas within the domain. Areas of apparently local production are also visible in satellite chlorophyll images, especially in areas very close to the coast and in the Shumagin Islands (see Fig. 10). Local areas in the Shelikof Strait and sea valley intensify, first in the northern areas of the Strait closer to Line 8, but also independently downstream at the same time. Later still, the highest numbers generally follow the flow pattern and the areas of high production are often more continuous. So it is possible and even likely that (chlorophyll and) nauplii are advected into the domain from the north within Shelikof Strait and the sea valley; however, it seems likely that local production, perhaps in nearshore areas and the Shumagin Islands, also has a role in producing naupliar prey for larval pollock.

Another persistent question about this stock of pollock is why the location and timing of spawning has been so consistently seen in central Shelikof Strait in early April. Hinckley *et al.* (2001) performed a model experiment using the walleye pollock IBM that indicated that this consistency of the spawning location and timing may be partially explained (in evolutionary terms) by transport processes taking young fish to nursery areas. The window of opportunity for spawning

times and locations that would result in successful transport to Shumagin Island nursery areas was March to July (spawning actually occurs primarily in April), and over an area extending somewhat to the northeast and southwest of central Shelikof Strait. This window was broader than that actually seen. It seems that factors other than physical transport alone must be important. These other factors could include the spatial and temporal availability of prey, the presence or absence of predators on the early life stages of pollock, and details of mesoscale or submesoscale circulation or other physical factors that were not captured by the hydrodynamic model.

NPZ model simulations of the distribution and timing of the production of *Pseudocalanus* spp. nauplii help us to further narrow this optimal window for spawning. There was a definite peak in naupliar production occurring in most modeled years between early May and early June (see also Napp *et al.*, 2005). If larvae were spawned early (e.g., mid-February), they would reach first-feeding in early March. At this time the increase in nauplii has not yet begun, and concentrations are significantly below the threshold level of 20 000 nauplii m^{-3} (20 L^{-1}) thought to be necessary in Shelikof for successful feeding and growth (Theilacker *et al.*, 1996). If larvae were spawned after mid-May, they would miss the peak of naupliar production. The observed spawning date (early to mid-April) results in first-feeding larvae in the water column in late April to mid-May, after naupliar production rises above the threshold level in most years, according to our model.

The spatial distribution of prey also helps to narrow the optimal spawning location. If pollock spawn in the northwest Shelikof sea valley, downstream of Line 8, they would be quickly carried into the coastal region between the Semidi and the Shumagin Islands, at times when naupliar abundances in this area are quite low. Fish spawned farther to the north and east, in Shelikof Strait proper, are more likely to remain in the sea valley, in areas of high prey abundance.

The consistent timing and location of spawning in Shelikof Strait then may have evolved as a response to the timing and location of prey production as well as transport. Spawning peaks around the first week of April in Shelikof Strait, but begins mid-March and continues until early May. Larvae spawned earlier than the peak of spawning may have difficulty finding food at the time of first feeding; however, those spawned in early May could reach first feeding in time to hit peak levels of naupliar biomasses (mid- to late May). This ensures a temporal match between larval pollock production and the production of their prey. Overall, the model provided both spatial and temporal evidence to support the match–mismatch theory (Cushing, 1972, 1974) for walleye pollock production in Shelikof Strait.

The delay of the 1989 modeled bloom and consequent low abundance of copepod nauplii until late in May may have been because 1989 was a very dry year (Table 1), with low freshwater runoff leading to weak water column stratification. The mixed layer depth in the model was deep until May, when runoff from rain and snow melt increased.

However, it remains unclear whether the model results for 1989, showing an anomalously late production of nauplii, truly represent what actually happened in that year. Data for comparison on biological variables were sparse; however, there is one data point showing an earlier bloom in this year, and two naupliar measurements that are higher than modeled concentrations (Fig. 3, DOY 121 and 128).

Canino *et al.* (1991) found between 12 500 and 26 000 nauplii m^{-3} in late April to mid-May 1989, levels similar to those found in the model output for this year, and also similar to those found by Incze *et al.* (1990) for 1987 (a low recruitment year). Canino *et al.* (1991) found that RNA/DNA levels in larval pollock were very low in 1989, indicating that the larvae were approaching starvation levels. They estimate that 39 000–58 000 nauplii m^{-3} would be needed to support normal pollock larval growth. This was a more typical level seen in model output for other years.

Finally, although originally 1989 was thought to be a very poor recruitment year (Megrey *et al.*, 1995), estimates of recruitment for that year have been revised upward based on data presented in Dorn *et al.*'s (2007) Table 1.18. It is, therefore, somewhat unclear whether 1989 was in fact a bad year.

As well as providing a source of insight into the spatial and temporal variability in prey resources for young walleye pollock in this region, this modeling work represents one of only two three-dimensional NPZ models designed to simulate dynamics in the Gulf of Alaska coastal regions that we know of (see also Hinckley *et al.*, in press, Hermann *et al.*, in press). We hope that what we have learned in this modeling effort will aid future modelers of this region.

This NPZ model adds a temporally and spatially variable prey resource to our set of coupled biophysical models focused on recruitment processes for pollock in the western Gulf of Alaska. As such, it has provided us with an insight into spatial and temporal processes affecting larval pollock feeding and recruitment, and provides evidence for the match–mismatch hypothesis for this stock.

ACKNOWLEDGEMENTS

This research is contribution FOCI-0501 to NOAA's Fisheries Oceanography Coordinated Investigations.

REFERENCES

Asselin, R. (1972) Frequency filter for time integrations. *Mon. Weather Rev.* **100:**487–490.

Bailey, K.M. (2000) Shifting control of recruitment of walleye pollock *Theragra chalcogramma* after a major climatic and ecosystem change. *Mar. Ecol. Prog. Ser.* **198:**215–224.

Bailey, K.M. and Ciannelli, L. (2007) Walleye pollock. Section 2.5.5. In: *Long-Term Ecological Change in the Northern Gulf of Alaska*. R.S. Spies (ed.) Amsterdam: Elsevier, pp. 85–93.

Bailey, K.M. and Spring, S.M. (1992) Comparison of larval, age-0 juvenile and age-2 recruit abundance indices of walleye pollock, *Theragra chalcogramma*, in the western Gulf of Alaska. *ICES J. Mar. Sci.* **49:**297–304.

Bailey, K.M. and Stehr, C.L. (1986) Laboratory studies on the early life history of the walleye pollock, *Theragra chalcogramma* (Pallas). *J. Exp. Mar. Biol. Ecol.* **99:**233–246.

Bibby, T.S., Gorbunov, M.Y., Wyman, K.W. and Falkowski, P.G. (2008) Photosynthetic responses to upwelling in mesoscale eddies in the subtropical North Atlantic and Pacific Oceans. *Deep Sea Res.* **55:**1310–1320.

Blood, D.M., Materese, A.C. and Yoklavich, M.M. (1994) Embryonic development of walleye pollock, *Theragra chalcogramma*, from Shelikof Strait, Alaska. *Fish. Bull.* **92:**207–222.

Bograd, S.J., Stabeno, P.J. and Schumacher, J.D. (1994) A census of mesoscale eddies in Shelikof Strait, Alaska, during 1989. *J. Geophys. Res.* **99:**18243–18254.

Canino, M.F., Bailey, K.M. and Incze, L.S. (1991) Temporal and geographic differences in feeding and nutritional condition of walleye pollock larvae *Theragra chalcogramma* in Shelikof Strait, Gulf of Alaska. *Mar. Ecol. Prog. Ser.* **79:**27–35.

Ciannelli, L., Chan, K-S, Bailey, K.M. and Stenseth, N.C. (2004) Nonadditive effects of the environment on the survival of a large marine fish population. *Ecology* **85:**3418–3427.

Corkett, J. and McLaren, I.A. (1978) The biology of *Pseudocalanus*. *Adv. Mar. Biol.* **15:**1–231.

Cushing, D.H. (1972) The production cycle and the numbers of marine fish. *Symp. Zool. Soc. London* **29:**213–232.

Cushing, D.H. (1974) The natural regulation of fish populations. In: *Sea Fisheries Research*. F.R. Harden Jones (ed.) London: Elek Science, pp. 399–412.

Dagg, M.J., Clarke, M.E., Nishiyama, T. and Smith, S.L. (1984) Production and standing stock of copepod nauplii, food items for larvae of walleye pollock *Theragra chalcogramma* in the southeastern Bering Sea. *Mar. Ecol. Prog. Ser.* **19:**7–16.

Davis, M.W. and Olla, B.L. (1992) Comparison of growth, behavior and lipid concentrations of walleye pollock *Theragra chalcogramma* larvae fed lipid-enriched, lipid-deficient and field-collected prey. *Mar. Ecol. Prog. Ser.* **90:**23–30.

Dorn, M., Aydin, K., Barbeaux, S. *et al.* (2007) Gulf of Alaska Walleye Pollock. In: *Stock Assessment and Fishery Evaluation Report for the Groundfish Resources of the Gulf of Alaska Region*. Anchorage: North Pacific Fishery Management Council, p. 118.

Eppley, R.W. (1972) Temperature and phytoplankton growth in the sea. *Fish. Bull. US* **70:**1063–1085.

Frost, B.W. (1987) Grazing control of phytoplankton stock in the open subarctic Pacific Ocean: a model assessing the role of mesozooplankton, particularly the large calanoid copepods *Neocalanus* spp. *Mar. Ecol. Prog. Ser.* **39:**49–68.

Frost, B.W. (1993) A modeling study of processes regulating plankton standing stock and production in the open subarctic Pacific Ocean. *Prog. Oceanogr.* **32:**17–56.

Haidvogel, D.B., Wilkin, J.L. and Young, R. (1991) A semi-spectral primitive equation ocean circulation model using vertical sigma and orthogonal curvilinear horizontal coordinates. *J. Comput. Phys.* **94:**151–185.

Haidvogel, D.B., Arango, H., Hedstrom, K., Beckmann, A., Malanotte-Rizzoli, P. and Shchepetkin, A. (2000) Model evaluation experiments in the North Atlantic Basin: simulations in non-linear terrain-following coordinates, 2000. *Dyn. Atmos. Oceans* **32:**239–281.

Haidvogel, D.B., Arango, H., Budgell, W.P. *et al.* (2008) Ocean forecasting in terrain-following coordinates: formulation and skill assessment of the Regional Ocean Modeling System. *J. Comput. Phys.* **227:**3595–3624.

Harrison, P.J., Whitney, F.A., Tsuda, A., Saito, J. and Tadokoro, K. (2004) Nutrient and plankton dynamics in the NE and NW gyres of the subarctic Pacific Ocean. *J. Oceangr.* **60:**93–117.

Hayward, T.L. and Mantyla, A.W. (1990) Physical, chemical and biological structure of a coastal eddy near Cape Mendocino. *J. Mar. Res.* **48:**825–850.

Herman, A.W. and Platt, T. (1983) Numerical modeling of diel carbon production and zooplankton grazing on the Scotian shelf based on observational data. *Ecol. Modell.* **18:**55–72.

Hermann, A.J. and Stabeno, P.J. (1996) An eddy resolving model of circulation on the western Gulf of Alaska shelf. I. Model development and sensitivity analysis. *J. Geophys. Res.* **101:**1129–1149.

Hermann, A.J., Hinckley, S, Megrey, B.A. and Stabeno, P.J. (1996) Interannual variability of the early life history of walleye pollock near Shelikof Strait as inferred from a spatially explicit, individual-based model. *Fish. Oceanogr.* **5**(Suppl. 1)**:**39–57.

Hermann, A.J., Hinckley, S., Megrey, B.A. and Napp, J.M. (2001) Applied and theoretical considerations for constructing spatially explicit individual-based models of marine fish early life history which include multiple trophic levels. *ICES J. Mar. Sci.* **58:**1030–1041.

Hermann, A.J., Hinckley, S., Dobbins, E.L. *et al.* (in press) Quantifying cross-shelf and vertical nutrient flux in the Coastal Gulf of Alaska with a spatially nested, coupled biophysical model. *Deep Sea Res. II*.

Hinckley, S., Hermann, A.J. and Megrey, B.A. (1996) Development of a spatially explicit, individual-based model of marine fish early life history. *Mar. Ecol. Prog. Ser.* **139:**47–68.

Hinckley, S., Hermann, A.J., Mier, K.L. and Megrey, B.A. (2001) The importance of spawning location and timing to successful transport to nursery areas: a simulation modeling study of Gulf of Alaska walleye pollock. *ICES J. Mar. Sci.* **58:**1042–1052.

Hinckley, S., Coyle, K.O., Gibson, G., Hermann, A.J. and Dobbins, E.L. (in press) A biophysical NPZ model with iron for the Gulf of Alaska: reproducing the differences between an oceanic HNLC ecosystem and a classical northern temperate shelf ecosystem. *Deep Sea Res. II*.

Hollowed, A., Ianelli, J.N. and Livingston, P.A. (2000) Including predation mortality in stock assessments: a case study for Gulf of Alaska walleye pollock. *ICES J. Mar. Sci.* **58:**279–293.

Incze, L.S. and Ainaire, T. (1994) Distribution and abundance of copepod nauplii and other small (40–300 μm) zooplankton during spring in Shelikof Strait, Alaska. *Fish. Bull. US* **92:**67–78.

Incze, L.S., Ortner, P.B. and Schumacher, J. D. (1990) Microzooplankton, vertical mixing and advection in a larval fish patch. *J. Plankton Res.* **12:**365–379.

Incze, L.S., Siefert, D.W. and Napp, J.M. (1997) Mesozooplankton of Shelikof Strait, Alaska: abundance and community abundance. *Cont. Shelf Res.* **17:**287–305.

Kendall, A.W. Jr, and Nakatani, T. (1992) Comparisons of early-life-history characteristics of walleye pollock *Theragra chalcogramma* in Shelikof Strait, Gulf of Alaska, and Funka Bay, Hokkaido, *Japan. Fish. Bull.* **90:**129–138.

Kendall, A.W. Jr, Clarke, M.E., Yoklavich, M.M. and Boehlert, G.W. (1987) Distribution, feeding and growth of larval walleye pollock, *Theragra chalcogramma*, from Shelikof Strait, Gulf of Alaska. *Fish. Bull. US* **85:**499–521.

Kendall, A.W. Jr, Perry, R.I. and Kim, S. (1996) Walleye pollock recruitment in Shelikof Strait: applied fisheries oceanography. *Fish. Oceanogr.* **5**(Suppl. 1)**:**4–18.

Kimura, S., Kasai, A., Nakata, H., Sugimoto, T., Simpson, J.H. and Cheok, J.V.S. (1997) Biological productivity of mesoscale eddies caused by frontal disturbances in the Kuroshio. *ICES J. Mar. Sci.* **54:**179–192.

Mahaffey, C., Benitez-Nelson, C.R., Bidigare, R.R., Yoshimi, R. and Karl, D.M. (2008) Nitrogen dynamics within a wind-driven eddy. *Deep Sea Res.* **55:**1398–1411.

Martin, J. H., Gordon, R. M., Fitzwater, S. and Broenkow, W.W. (1989) VERTEX: phytoplankton/iron studies in the Gulf of Alaska. *Deep-Sea Res. I* **6:**649–680.

McKay, M.D., Beckman, R.D. and Conover, W.J. (1979) A comparison of three methods for selecting values of input variables in the analysis of output from computer code. *Technometrics* **21:**239–245.

Megrey, B.A. and Hinckley, S. (2001) The effect of turbulence on feeding of larval fishes: a sensitivity analysis using an individual-based model. *ICES J. Mar. Sci.* **58:**1015–1029.

Megrey, B.A., Bograd, S.J., Rugen, W.C. *et al.* (1995) An exploratory analysis of associations between biotic and abiotic factors and year-class strength of Gulf of Alaska walleye pollock (*Theragra chalcogramma*). In: *Climate Change and Northern Fish Populations*. R.J. Beamish (ed.) *Can. Spec. Publ. Fish. Aquat. Sci* **121:** 227–243.

Merrick, R.L., Chumbley, M.K. and Byrd, G.V. (1997) Diet diversity of Steller sea lions (*Eumetopias jubatus*) and their population decline in Alaska: a potential relationship. *Can. J. Fish. Aquat. Sci.* **54:**1342–1348.

Napp, J.M., Incze, L.S., Ortner, P.B., Siefert, D.L.W. and Britt, L. (1996) The plankton of Shelikof Strait, Alaska: standing stock, production, mesoscale variability and their relevance to fish survival. *Fish. Oceanogr.* **5**(Suppl. 1)**:**19–38.

Napp, J.M., Kendall, A.W. . Jr and Schumacher, J.D. (2000) A synthesis of biological and physical processes affecting the feeding environment of larval walleye pollock (*Theragra chalcogramma*) in the eastern Bering Sea. *Fish. Oceangr.* **9:**147–162.

Napp, J.M., Hopcroft, R.R., Baier, C.T. and Clarke, C. (2005) Distribution and species-specific egg production of *Pseudocalanus* in the Gulf of Alaska. *J. Plankton Res.* **27:**415–426.

Parsons, T.R., Takahashi, M. and Hargrave, B. (1977) *Biological Oceanographic Processes*, 2nd edn. Oxford: Pergamon Press.

Redfield, A.C., Ketchum, B.H. and Richards, F.A. (1963) The influence of organisms on the composition of seawater. In: *The Sea*, M.N. Hill (ed.) New York: Wiley Interscience, pp. 26–77.

Reed, R.K., Schumacher, J.D. and Incze, L.S. (1987) Circulation in Shelikof Strait, Alaska. *J. Phys. Oceanogr.* **17:**1546–1554.

Royer, T.C. (1982) Coastal freshwater discharge in the northeast Pacific. *J. Geophys. Res.* **87:**2017–2021.

Siefert, D.L.W. and Incze, L.S. (1989) *Zooplankton of Shelikof Strait, Alaska, April to July 1987: Data from Fisheries-Oceanography Coordinated Investigations (FOCI) Cruises*. NWAFC Proceedings Report 89-22. Seattle: Alaska Fisheries Science Center.

SOLMET (1979) *Hourly Solar Radiation – Surface Meteorological Observations*. SOLMET Vol. 1. Final Report TD-9724. Asheville, NC: National Climatic Center.

Stabeno, P.J. and Hermann, A.J. (1996) An eddy resolving model of circulation on the western Gulf of Alaska shelf. II. Comparison of results to oceanographic observations. *J. Geophys. Res.* **101:**1151–1161.

Stabeno, P.J., Hermann, A.J., Bond, N.A. and Bograd, S.J. (1995) Modeling the possible impact of climate change on the survival of larval walleye pollock (*Theragra chalcogramma*) in the Gulf of Alaska. In: *Climate Change and Northern Fish Populations*. R.J. Beamish (ed.) *Can. Spec. Publ. Fish. Aquat. Se.* **121:** 719–727.

Stabeno, P.J., Schumacher, J.D., Bailey, K.M., Brodeur, R.D. and Cokelet, E.D. (1996) Observed patches of walleye pollock eggs and larvae in Shelikof Strait, Alaska: their characteristics, formulation and persistance. *Fish. Oceanogr.* **5**(Suppl. 1)**:**81–91.

Stabeno, P.J., Bond, N.A., Hermann, A.J., Kachel, N.B., Mordy, C.W. and Overland, J.E. (2004) Meteorology and oceanography of the Northern Gulf of Alaska. *Cont. Shelf Res.* **24:**859–897.

Strom, S. L., Miller, C. B. and Frost, B. W. (2000) What sets lower limits to phytoplankton stocks in high nitrate, low-chlorophyll regions of the open ocean? *Mar. Ecol. Prog. Ser.* **193:**19–31.

Strom, S.L., Olson, M.B., Macri, E.L. and Mordy, C.W. (2007) Cross-shelf gradients in phytoplankton community structure, nutrient utilization, and growth rate in the northern coastal Gulf of Alaska. *Mar. Ecol. Prog. Ser.* **328:**75–92.

Theilacker, G.H., Bailey, K.M., Canino, M.F. and Porter, S.M. (1996) Variations in larval walleye pollock feeding and condition: a synthesis. *Fish. Oceanogr.* **5**(Suppl. 1)**:**112–123.

Werner, F.E., Quinlan, J.A., Lough, R.G. and Lynch, D.R. (2001) Spatially-explicit individual based modeling of marine populations: a review of the advances in the 1990s. *Sarsia* **86:**411–421.

APPENDIX 1

Notation used for state variables and subscripts in model equations.

Subscripts

z	Depth (m)
MLD	Mixed layer depth (m)
i	Zooplankton (herbivore) species (*Neocalanus*, spp. or *Pseudocalanus*, spp. or stage (of *Pseudocalanus*, spp.), used with H
θ_z	Temperature at depth z (°C)
X_{MLD}	Average concentration of state variable (where $X = N$ or P) in the mixed layer, where MLD = mixed layer depth in meters
$X_{\mathrm{MLD+1}}$	Concentration of state variable (where $X = N$ or P), where depth = MLD + 1 meters
X_z	Concentration of state variable (where $X = N$ or P) in the stratified layer where z = depth in meters at current location
X_{z+1}	Concentration of state variable (where $X = N$ or P) in the stratified layer where depth = z + 1 meters
X_{z-1}	Concentration of state variable (where $X = N$ or P) in the stratified layer where depth = z−1 meters
$H_{i,\mathrm{MLD}}$	Concentration of herbivore species or stage i, where $i = 1,\ldots,14$ (see below under State Variables), in the mixed layer
$H_{\mathrm{MLD+1}}$	Concentration of herbivore species or stage i, where depth = MLD + 1 meters
$H_{i,z}$	Concentration of herbivore species or stage i, in the stratified layer where z = depth in meters at current location
$H_{i,z+1}$	Concentration of herbivore species or stage i, in the stratified layer where depth = z + 1 meters
$H_{i,z\text{-}1}$	Concentration of herbivore species or stage i, in the stratified layer where depth = z−1 meters

State variables

State variable (Units)	Definition
N (mmol N m^{-3})	Nutrient (nitrate) concentration
P (mg C m^{-3})	Phytoplankton concentration
H_i (mg C m^{-3} or n m^{-3})	Zooplankton herbivore species or stage concentration where, i = 1 (*Neocalanus*, spp.), 2 (*Pseudocalanus*, spp. *eggs*), 3,…,4 (*Pseudocalanus* spp. N1 and N2, nonfeeding nauplii), 5,…,8 (*Pseudocalanus* spp. N3 – N6, feeding nauplii), 9,…,13 (*Pseudocalanus* spp. C1 – C5, copepodites), 14 (*Pseudocalanus* spp. C6, adults)

APPENDIX 2

Governing equations for the biological model. Advection and diffusion terms are not included for clarity. Variable notation and subscripts are explained in Appendix 1. Parameter notation, values and sources are listed in Appendix 3a,b. Refer to Eqns 1 or 2 for the appropriate (mixed layer or stratified layer) mixing term.

Phytoplankton

(Mixed layer)

$$\frac{dP_{\mathrm{MLD}}}{dt} = \frac{1}{\mathrm{MLD}} \int_{z=0}^{\mathrm{MLD}} P_{\mathrm{MLD}} P_{\max} \tanh\left(\frac{\alpha \mathrm{PAR}_z}{P'_{\max}}\right) \left(\frac{N_{\mathrm{MLD}}}{d + N_{\mathrm{MLD}}}\right) dz - \sum_{i=1}^{i=14} \frac{e_i P_{\mathrm{MLD}} H_{i,\mathrm{MLD}}}{f_i + P_{\mathrm{MLD}}} + \mathrm{Mixing} \quad (A1)$$

(Stratified layer)

$$\frac{dP_z}{dt} = P_z P_{\max} \tanh\left(\frac{\alpha \mathrm{PAR}_z}{P'_{\max}}\right) \left(\frac{N_z}{d + N_z}\right) - \sum_{i=1}^{i=14} \frac{e_i P_z H_{i,z}}{f_i + P_z} + \mathrm{Mixing} \quad (A2)$$

Phytoplankton was modeled as a single compartment, as there were no size-structured data for this region at the time this model was developed. Uptake of nutrients was modeled as a function of light and nutrients. Photosynthetically active radiation (PAR) as a function of depth (PAR_z) was modeled according to Frost (1987),

$$\mathrm{PAR}_z = 0.5 I_z \quad (A3)$$

where irradiance (I_z) was a function of depth (z) in meters (m) and an extinction coefficient (t),

$$I_z = I_0 e^{-\int t dz} \quad (A4)$$

where $t = 0.07 + 0.12 P_{\mathrm{chl}\text{-}a}$ (Herman and Platt, 1983).

Light at the surface was provided by daily climatological incident solar radiation (Appendix 4). The radiation climatology did not include interannual differences due to variability in cloud cover in the region.

The maximum rate of photosynthesis $P_{\max}$, was calculated from the temperature-controlled doubling rate and the number of hours of daylight:

$$P_{\max} = (e^{D \ln 2} - 1.0) \frac{\mathrm{DL}}{24} \quad (A5)$$

The doubling rate, D, was modeled as in the empirical formula of Eppley (1972) relating doubling rate to temperature, and was modified by day length (DL) in hours.

$$D = 0.85\ (10)^{0.0275\theta} \quad \text{where } \theta_z = \text{temperature at depth } z\ (^\circ\text{C}) \qquad (A6)$$

Temperature in the model was advected and diffused relative to climatology, in the same manner as salinity (see Hermann and Stabeno, 1996 for details). Mean vertical profiles of temperature for March and October were obtained from the data of Reed *et al.* (1987); these profiles were linearly interpolated in time to provide the depth- and time-dependent (but horizontally uniform) climatological background for the diffusion term.

The chlorophyll-specific maximum rate of photosynthesis ($P'_{\max}$) was equal to $P_{\max}$ times the carbon-to-chlorophyll ratio (c), i.e., $P'_{\max} = c \cdot P_{\max}$. Grazing losses were modeled as the sum of the uptake by all herbivores.

Zooplankton

Major grazer (Neocalanus spp.)
(Mixed layer)

$$\frac{dH_{1,\mathrm{MLD}}}{dt} = \frac{\gamma_1 e_1 P_{\mathrm{MLD}}}{f_1 + P_{\mathrm{MLD}}} H_{1,\mathrm{MLD}} - m_1 H_{1,\mathrm{MLD}} + \text{Mixing} \qquad (A7)$$

(Stratified layer)

$$\frac{dH_{1,z}}{dt} = \frac{\gamma_1 e_1 P_z}{f_1 + P_z} H_{1,z} - m_1 H_{1,z} + \text{Mixing} \qquad (A8)$$

A large copepod (H_1), which is not a food item for larval pollock, was included in the model as a major grazer, and was parameterized as *Neocalanus* spp., the dominant copepod by biomass in this region. The species of *Neocalanus* represented were *Neocalanus plumchrus* and *Neocalanus flemingerii*. The population dynamics of *Neocalanus* spp. was aggregated, with no stage structure. In the model, *Neocalanus* spp. had only one generation per year, and its growth was independent of temperature. Grazing was modeled with a Michaelis–Menton function, and natural mortality as a simple linear function using a constant daily mortality rate. To simulate the onset of diapause in late spring and early summer, *Neocalanus* spp. were removed from the water column over a period of a month, starting at DOY 150 (ca. the end of May), by applying an arctangent function to the biomass (not shown).

Larval pollock prey (Pseudocalanus spp.)
The species of *Pseudocalanus* used in this model were *Pseudocalanus newmani*, *Pseudocalanus mimus*, *Pseudocalanus moultani* and *Pseudocalanus minutus* (Napp *et al.*, 2005). Although responses of these four species may vary with environmental conditions, for simplicity we modeled them as one group. The stage-structured biomass of *Pseudocalanus* spp. was modeled because its egg (H_2), six naupliar (H_3–H_8) and six copepodite (H_9–H_{14}) stages are a major portion of the diet of larval pollock (Dagg *et al.*, 1984; Kendall *et al.*, 1987; Canino *et al.*, 1991; Napp *et al.*, 1996). The proportion of each stage eaten by larval pollock varies with larval length (Kendall *et al.*, 1987).

Stage biomasses are modeled as a (egg stage) hatch rate or (non-egg stage) transfer rate from the next earlier stage, minus transfer to the next higher stage, minus mortality plus diffusion. Stage-specific equations are given below.

1. Eggs (H_2)
(Mixed layer)

$$\frac{dH_{2,\mathrm{MLD}}}{dt} = a\varepsilon H_{14,\mathrm{MLD}} \frac{dwt_2}{dwt_{14}} - \tau_2 H_{2,\mathrm{MLD}} - m_2 H_{2,\mathrm{MLD}} + \text{Mixing} \qquad (A9)$$

(Stratified layer)

$$\frac{dH_{2,z}}{dt} = a\varepsilon H_{14,z} \frac{dwt_2}{dwt_{14}} - \tau_2 H_{2,z} - m_2 H_{2,z} + \text{Mixing} \qquad (A10)$$

In the model, *Pseudocalanus* spp. egg production (ε) was a function of phytoplankton carbon,

$$\varepsilon = er \cdot emax, \qquad (A11)$$

where er = 1.0 if phytoplankton carbon > 200.0 mg m^{-3}, and otherwise $er = 0.005P$. Hatching was assumed to be continuous, for simplicity. The hatch rate of eggs (τ_2) was a function of temperature and the egg stage duration (dur_2)

$$\tau_2 = \frac{1}{dur_2} = b_2(\theta_z + 11.45)^{-2.05} \quad \text{(Corkett and McLaren, 1978)} \qquad (A12)$$

2. Nonfeeding stages (H_i where i = 3, 4)
(Mixed layer)

$$\frac{dH_{i,\mathrm{MLD}}}{dt} = \tau_{i-1} H_{i-1,\mathrm{MLD}} - \tau_i H_{i,\mathrm{MLD}} - m_i H_{i,\mathrm{MLD}} + \text{Mixing} \qquad (A13)$$

(Stratified layer)

$$\frac{dH_{i,z}}{dt} = \tau_{i-1}H_{i-1,z} - \tau_i H_{i,z} - m_i H_{i,z} + \text{Mixing} \quad (A14)$$

Naupliar stages N1 and N2 of *Pseudocalanus*, spp. are nonfeeding. The coefficients of transfer between stages i and $i + 1$ (τ_i) for post-egg stages were the inverse of each stage duration (dur_i), which were themselves functions of the egg stage duration (dur_2) (Corkett and McLaren, 1978):

$$\tau_i = \frac{1}{dur_i} \quad (A15)$$

$$\text{where } dur_i = b_i(dur_2). \quad (A16)$$

3. Feeding stages (H_i where $i = 5,\ldots,14$)
(Mixed layer)

$$\frac{dH_{i,\text{MLD}}}{dt} = \tau_{i-1}H_{i-1,\text{MLD}} + \frac{\gamma_i e_i P_{\text{MLD}}}{f_i + P_{\text{MLD}}}H_{i,\text{MLD}} - m_i H_{i,\text{MLD}} - \tau_i H_{i,\text{MLD}} + \text{Mixing} \quad (A17)$$

(Stratified layer)

$$\frac{dH_{i,z}}{dt} = \tau_{i-1}H_{i-1,z} + \frac{\gamma_i e_i P_z}{f_i + P_z}H_{i,z} - m_i H_{i,z} - \tau_i H_{i,z} + \text{Mixing} \quad (A18)$$

Naupliar stages N3 through N6, and all copepodite stages (C1 through C6) feed actively; feeding was modeled with a Michaelis–Menton algorithm. Biomass of each stage was converted to numbers using a dry weight to carbon ratio (*conv*) and dry weights per individual for each stage (dwt_i).

Nutrients

(Mixed layer)

$$\frac{dN_{\text{MLD}}}{dt} = -\frac{\xi}{\text{MLD}}\int_{z=0}^{\text{MLD}} P_{\text{MLD}}P_{\max}\tanh\left(\frac{\alpha \text{PAR}_z}{P'_{\max}}\right) \times \left(\frac{N_{\text{MLD}}}{d + N_{\text{MLD}}}\right)dz + \sum_{i=1}^{i=14}(1-\gamma_{H_i})\frac{e_i P_{\text{MLD}}H_{i,\text{MLD}}}{f_i + P_{\text{MLD}}} + \text{Mixing} \quad (A17)$$

(Stratified layer)

$$\frac{dN_z}{dt} = -\xi P_z P_{\max}\tanh\left(\frac{\alpha \text{PAR}_z}{P'_{\max}}\right)\left(\frac{N_z}{d + N_z}\right) + \sum_{i=1}^{i=14}(1-\gamma_{H_i})\frac{e_i P_z H_{i,z}}{f_i + P_z} + \text{Mixing} \quad (A18)$$

Nutrients (nitrate) were modeled as a single compartment and were supplied to the upper layers through vertical mixing from a deep nutrient pool, and horizontally from the upstream boundary conditions. Phytoplankton uptake (Eqns A.1 and A.2) was subtracted, and herbivore excretion summed over all species and stages was added to the nitrate concentration.

APPENDIX 3A

Parameter definitions, values and sources for the NPZ model. Parameters marked * are optimized parameters. Numbers in parentheses under 'Source' for these parameters are the range of values for the parameter which resulted in model output that fell within the range of the observed data.

Name	Definition	Value	Source
ξ	N:C ratio (mmol N mg C^{-1})	0.0126	Redfield *et al.* (1963)
k_v	Vertical eddy diffusivity (m^2 day^{-1})	1.0	Hermann and Stabeno (1996)
conv	Dry W:C conversion factor	0.4	Parsons *et al.* (1977)
c	Phytoplankton C:Chl-*a* ratio	55.0	Frost (1993)
α	Photosynthetic efficiency (mg C (mg Chl-a)$^{-1}$ (E m^{-2})$^{-1}$)	21.0	Frost (1993)
d	Half-saturation constant for N uptake by P (mmol N m^{-3})	1.0	Frost (1987, 1993)
γ_1	Growth efficiency for *Neocalanus* spp.	0.522*	(0.5–0.547)
m_1	Mortality rate for *Neocalanus* spp. (day^{-1})	0.0048*	(0.0048–0.0096)
e_1	*Neocalanus* spp. max. specific ingestion rate (mg C (mg C)$^{-1}$$d^{-1}$)	0.166*	(0.155–0.166)
f_1	*Neocalanus* spp. half-saturation constant for ingestion (mg C m^{-3})	45.69*	(45.395–48.0)

APPENDIX 3B

Stage-specific parameters for *Pseudocalanus* spp. Parameters marked * are optimized parameters. Numbers in parentheses for these parameters are the range of values for the parameter that resulted in model output that fell within the range of the observed data.

Name	Definition	Egg	N1	N2	N3	N4	N5	N6	C1	C2	C3	C4	C5	Adult	Source
a	Proportion of adult female *Pseudocalanus* spp.													0.667	Siefert and Incze (1989)
emax	Max. *Pseudocalanus* eggs female^{-1} day^{-1}													5.0	Corkett and McLaren (1978)
γ_i (i = 5,…,14)	Growth efficiency for *Pseudocalanus* spp.				0.19*	0.19*	0.19*	0.19*	0.19*	0.19*	0.19*	0.19*	0.19*	0.19*	(0.156–0.195)
e_i (i = 5,…,8)	*Pseudocalanus* spp. naupliar max. specific ingestion rate (mg C mg Chl-a^{-1} day^{-1}) for stage i				3.65*	3.65*	3.65*	3.65*							(3.514–3.952)
f_i (i = 5,…,8)	*Pseudocalanus* spp. naupliar half-saturation constant for ingestion (mg C m^{-3}) for stage i				67.31*	67.31*	67.31*	67.31*							(50.84–67.31)
e_i (i = 9,…,13)	*Pseudocalanus* spp. copepodite max. specific ingestion rate (mg C mg Chl-a^{-1} day^{-1}) for stage i								3.48*	3.48*	3.48*	3.48*	3.48*		(3.242–3.478)
f_i (i = 9,…,13)	*Pseudocalanus* spp. copepodite half-saturation constant for ingestion (mg C m^{-3})								28.29*	28.29*	28.29*	28.29*	28.29*		(26.245–33.535)
e_{14}	*Pseudocalanus* spp. adult max. specific ingestion rate (mg C mg Chl-a^{-1} day^{-1})													2.53*	(2.526–2.705)
f_{14}	*Pseudocalanus* spp. adult half-saturation constant for ingestion (mg C m^{-3})													57.43*	(57.425–73.85)

APPENDIX 3B Continued.

Name	Definition	Egg	N1	N2	N3	N4	N5	N6	C1	C2	C3	C4	C5	Adult	Source
b_i (i = 2,…,14)	*Pseudocalamus* spp. stage duration coefficient	1845.0	0.18	0.37	1.46	0.81	0.69	0.4	1.23	1.00	0.98	1.02	1.32	8.00	Corkett and McLaren (1978)
m_i (i = 2,…,14)	*Pseudocalamus* spp. mortality per day	0.58 (0.51–0.58)	0.55 (0.5–0.59)	0.46 (0.46–0.53)	0.45 (0.45–0.51)	0.31 (0.21–0.34)	0.52 (0.52–0.58)	0.48 (0.39–0.48)	0.54 (0.54–0.57)	0.38 (0.32–0.44)	0.45 (0.33–0.45)	0.44 (0.40–0.46)	0.54 (0.48–0.54)	0.59 (0.50–0.6)	
dwt_i (i = 2,…,14)	Dry weight (mg) of stage i of *Pseudocalamus* spp.	$7.0e^{-5}$	$8.0e^{-5}$	$8.0e^{-5}$	$1.8e^{-4}$	$2.7e^{-4}$	$4.0e^{-4}$	$6.4e^{-4}$	$7.2e^{-4}$	$1.2e^{-3}$	$2.0e^{-3}$	$3.4e^{-3}$	$6.0e^{-3}$	$8.0e^{-3}$	Incze *et al.* (1997)

APPENDIX 4

Physical forcing and initial conditions for the SPEM-NPZ model.

Forcing	Source
Runoff	Monthly time series (Royer, 1982; Old Dominion University, unpubl. data)
Wind	Time-variable (12-hourly), derived from Fleet Numerical Oceanographic Center modeled geostrophic winds.
MLD	Derived from hydrodynamic model salinity profiles. Depth where the salinity was 0.05 psu greater than the surface value.
Temperature	Horizontally averaged CTD data for 1985 (Reed *et al.*, 1987). Depth profiles for March and October used as endpoints for linear interpolation according to date, to obtain mean temperature by time and date.
Daily incident solar radiation	Climatological time series from National Weather Service's Kodiak, Alaska weather station (SOLMET, 1979). Mean daily value (I_0, E m^{-2} day^{-1}).
Initial conditions	Data collected by NOAA's Fisheries Oceanography Coordinated Investigations (FOCI). Most from Line 8 (Fig. 1) (Incze and Ainaire, 1994; Napp *et al.*, 1996; Incze *et al.*, 1997).